Journal of Materials Chemistry A

Resolving buried optoelectronic features in metal halide perovskites via modulation spectroscopy studies

Journal:	*Journal of Materials Chemistry A*
Manuscript ID	TA-REV-08-2021-006484.R1
Article Type:	Review Article
Date Submitted by the Author:	24-Sep-2021
Complete List of Authors:	Amerling, Eric; University of Utah, Chemistry Hansen, Kameron; University of Utah, Chemistry Whittaker-Brooks, Luisa; University of Utah, Chemistry

ARTICLE

Resolving buried optoelectronic features in metal halide perovskites via modulation spectroscopy studies

Received 00th January 20xx,
Accepted 00th January 20xx

DOI: 10.1039/x0xx00000x

Eric Amerling,[a,b] Kameron Hansen,[a,b] and Luisa Whittaker-Brooks*[a]

As research on both bulk and low dimensional metal halide perovskites (MHPs) continues to grow, the tools necessary to gain insights into their exotic and highly convoluted optoelectronic features must also expand. Electroabsorption (EA) is a modulation spectroscopy technique that is exceptionally valuable at deconvoluting overlapping spectral features as well as discerning between different electronic environments in semiconductors. This review outlines the critical shortcomings of traditional optical spectroscopy has in determining essential properties such as the bandgap and exciton binding energy. We provide a brief overview of the working principles of EA, focusing on the differences between bound and unbound charge carriers that result in unique behavior when interacting with an applied electric field. We discuss key studies highlighting the unique characterizations available when coupling EA spectroscopy with traditional steady-state optical tools to investigate interesting and complex optical features in MHPs. We conclude that EA is a crucial tool for pushing the boundaries of our understanding of the optoelectronic properties of MHP thin films. When other optical characterizations fall short in the richness of data provided, EA can bridge the knowledge gap to provide a complete optoelectronic characterization of novel MHPs and deepen the understanding of current structures and compositions as a function of their structural and morphological dimensionality.

Introduction

A feature of metal halide perovskites (MHPs) that is vital to their performance success is their tunable optoelectronic properties.[1] However, this flexibility comes at the cost of complexity, both structurally and optically. From an optical perspective, distinguishing between different charge carrier types, continuum vs. excitonic features, or precisely identifying a critical state's energy can be very challenging due to the complex absorption broadening mechanisms which result from the dynamic activity of the MHP lattice.[2-4] To properly investigate some of the optical features in MHPs, traditional optical characterization tools such as absorption and photoluminescence spectroscopies must be complemented with more comprehensive optical techniques that can provide fingerprint signatures pertaining to convoluted exciton and bandgap features. Modulation spectroscopy, specifically electroabsorption (EA), yields derivative-like spectral features that provide much richer information on the nature of the absorbing states within semiconducting materials. As such, EA is a powerful tool for the investigation of many different properties in MHP thin film and crystals, including ion migration,[5-7] degradation mechanisms,[8] charge carrier interactions,[9] exciton reduced mass measurements,[10] dielectric confinement effects,[11] and most commonly, fundamental electronic properties such as exciton binding and bandgap energies.[12-22] EA spectroscopy is routinely left out of the toolbox of characterization techniques used to understand materials properties, and we believe it is underutilized within the MHP community.[23] This review highlights some of the challenges faced when using traditional optical spectroscopy characterization in the study of MHP materials. We also briefly review the fundamental mechanism of EA spectroscopy and present applications where this tool has been critical for understanding the optoelectronic features of MHPs.

Challenges associated with traditional spectroscopic characterization tools

The accurate determination of the optical properties of MHPs is of paramount importance for their future optoelectronic device applications. Unfortunately, there is considerable variability in the optical properties of MHPs reported in the literature. Tian *et al.* investigated the effects that the optical technique (ordinary spectrometer, integrating sphere, and a microscopy-based approach), film thickness, surface coverage, and surface scattering have on elucidating the absorption characteristics of methylammonium lead iodide ($MAPbI_3$) perovskite thin films.[24] When comparing the optical technique, the team found that using an ordinary spectrometer to characterize the absorption of $MAPbI_3$ thin films yield significant differences that are highly susceptible to variations in film coverage (**Figure 1A**). To circumvent this issue, the authors proposed the standardization of an ordinary spectrometer coupled with an integrating sphere. Such modification significantly increases the band-edge's sharpness by better accounting for scattering effects but grossly flattens the spectra in the UV region of the spectrum. Moreover, it is found that the classic featureless, flat, step-like absorption spectrum of $MAPbI_3$ is strongly dependent on the film quality (coverage, scattering coefficient, and thickness) as opposed to being dependent on the optoelectronic properties of the absorber. For example, as depicted in **Figure 1B**, by merely changing the thin film coverage, defined as the ratio of area covered by $MAPbI_3$ versus the substrate's total area, it is possible to artificially alter the optical density below 500 nm by almost an order of magnitude. This change in optical density is also found to be heavily dependent on light scattering. Given the likelihood of

[a] Department of Chemistry, University of Utah, Salt Lake City, UT 84112, USA
[b] These authors contributed equally to this work
*Corresponding Email: luisa.whittaker@utah.edu

over/underestimating the absorption properties of $MAPbI_3$ thin films when using traditional absorption spectroscopy, extreme care needs to be taken to account for artifacts that can radically change the shape and location of key optoelectronic features. Therefore, a consistent probe of the optoelectronic features of MHPs is necessary to avoid irreproducibility in photovoltaic device design and efficiency.

Given that EA is a modulation-based spectroscopy technique, physical artifacts, such as surface states or reflections, that can adversely affect the extracted optical properties do not impact the measurements acquired using this technique. The misrepresentation of surface states that lead to exotic optical features in MHPs can play a critical role in photovoltaic device design and could lead to device efficiency miscalculations. In the next section, we will highlight challenges in determining specific optoelectronic properties (e.g., bandgap and exciton resonance energy) as they also play an important role in the future of MHP applications.

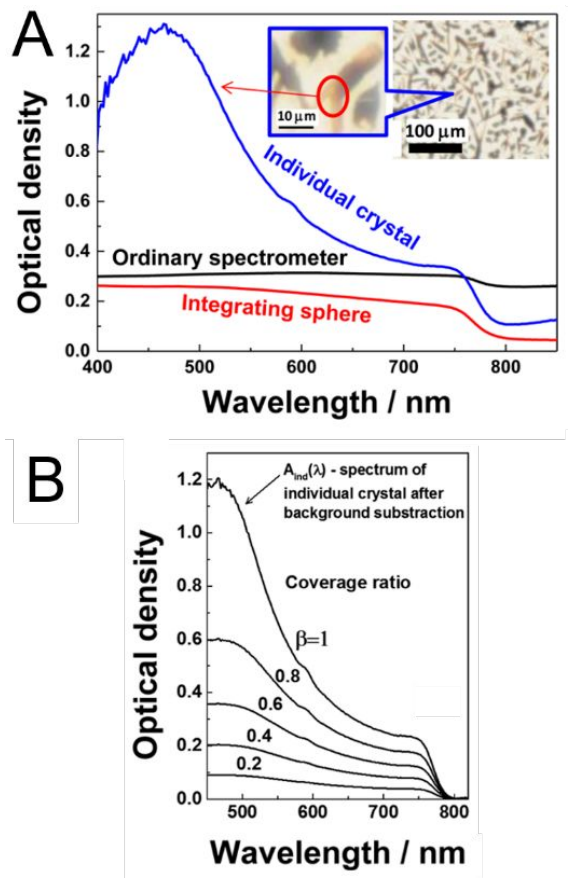

Figure 1. (A) Absorption spectrum for a $MAPbI_3$ thin film acquired using an ordinary spectrometer, an integrating sphere, and a microscope. Inset: micrographs showing the crystal under investigation. **(B)** Change in optical density due to coverage ratio (β) of $MAPbI_3$. Reproduced with permissions from *J. Phys. Chem. Lett.* 2015, 6, 17, 3466–3470 (ref. 24). Copyright 2015 American Chemical Society.[24]

Determining the bandgap of MHPs

The bandgap of a semiconductor (E_g) can be experimentally determined through absorption spectroscopy in a method developed by Tauc in 1966,[25] which was further developed by Davis and Mott.[26] The Tauc method is based on the relationship:[27]

$$(\alpha \cdot h\nu)^n = B(h\nu - E_g) \quad (1)$$

where α is the energy-dependent absorption coefficient, h is the Planck constant, ν is the photon's frequency, B is a constant, and E_g is the bandgap. n accounts for the type of electron transition; for direct bandgaps, $n = 2$, and for indirect bandgaps, $n = \frac{1}{2}$. By plotting a linear fit of the steep bandgap onset of α in a "$(\alpha \cdot h\nu)^n$ vs. $h\nu$" plot, the bandgap is extrapolated from the x-axis intercept.[28,29] However, a few fundamental assumptions are often made that add significant uncertainty to the E_g value extracted for direct bandgap materials. First, electron-hole Coulomb interactions are not taken into account, which, at lower temperatures, can cause an enhancement of α, therefore modifying the steepness of the E_g and the resulting x-axis intercept. Second, defect states and impurities that absorb below the E_g are often neglected. Third, the Tauc method assumes a parabolic-like band structure shape that is valid only at minimum energy, $\vec{k} \approx 0$, which is not applicable at high excitation energies $(h\nu \gg E_g)$ or in certain types of crystal structures.[29,30] Lastly, MHPs often exhibit above-gap absorption peaks which arise from the exciton's continuum of states overlapping with secondary VB/CB band minima.[31] When present, these peaks obfuscate the band-to-band transition and render the Tauc method ineffective. Thus, when selecting and justifying the region for linear fit analysis for constructing a Tauc plot from the absorption spectra, one must assign the area of the spectrum that will most accurately represent the absorption onset, which is often non-trivial. This can be seen in the Tauc plot constructed from the absorption of butylammonium lead iodide [$(CH_3(CH_2)_3NH_3)_2PbI_4$; also known as $(BA)_2PbI_4$] thin films displayed in **Figure 2**. This spectrum contains two dominant features i.e., the exciton peak at 2.43 eV and the absorption edge onset beginning at ~2.60 eV. The dotted linear regression lines represent the fits of three different regions. The red line fits well (R^2 = 0.99) to the upper portion of the absorption onset, while the green line fits well (R^2 = 0.99) to the lower portion of the absorption onset. The blue line has the poorest fit (R^2 = 0.92) along the middle part of the absorption onset. The labelled energies are the X-intercepts, representing the predicted bandgap from the Tauc plot. By selecting different linear regions based on the absorption onset, the extrapolated E_g value varies by 0.22 eV. This is an issue that does not have a robust fundamental solution and the choice of the linear region is commonly placed on the individual researcher.

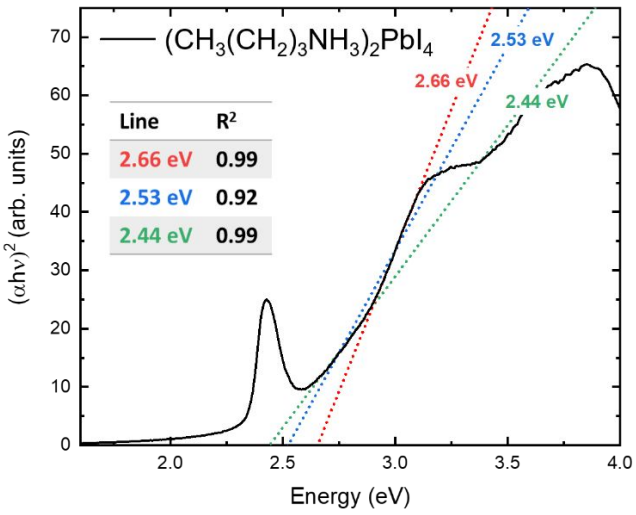

Figure 2. Tauc plot for $(BA)_2PbI_4$ thin films with three distinct regions chosen for linear fit analysis.

Another source of error in analyzing the absorption features using a Tauc plot is the lack of "sharpness" in the absorption edge. In thin film samples, low energy sub-gap states cause large, exponential tails in the absorption, known as Urbach tails.[32,33] Urbach tails are indicative of structurally disordered, amorphous, or poorly crystalline phases within a thin film and are common in MHPs.[34] Similarly, surface roughness can cause significant scattering errors in the absorption edge onset location and, therefore, adversely affect how the resulting plot is analyzed. Finally, Tauc plots do not account for the overlap of excitonic features and band-to-band transitions.[12,28] In polycrystalline MHP thin films, exciton absorption resonances can be strongly broadened, especially at room temperature, and are often merged with the continuum states in the absorption due to surface artifacts and phonon scattering.[35] This significantly complicates the accurate determination of E_g in MHPs.[12,36] While the E_g of an MHP determines the range of light that can be utilized in a photovoltaic device, the exciton binding energy determines whether excited charges exist as bound excitons or free carriers at room temperature. This exciton binding energy factor has considerable implications on the function of solar cell devices. The following section will discuss how the exciton binding energy value is determined with traditional optical spectroscopy and how it could be miscalculated.

Determining the exciton binding energy of MHPs

When a photon with energy equal to or higher than the bandgap is absorbed in a semiconductor, an electron-hole pair, or exciton, is typically formed. This quasiparticle is held together by attractive Coulomb interactions determined by the dielectric environment surrounding the exciton and is known as the exciton binding energy (E_b).[37,38] The Wannier–Mott exciton model, which is generally the model accepted for explaining charge carrier interactions in 3D MHPs, is described by the *n*th excitonic resonance (E_n) in terms of the hydrogen model:

$$E_n = E_g - \frac{Ry}{n^*} \quad (2)$$

where E_g is the bandgap, Ry is the Rydberg energy constant, and n* is the excitonic level. Ideally, E_b can be experimentally measured by resolving the energy separation of the Rydberg series (n = 1, 2, etc.) in the absorption spectrum.[36] However, even for high quality MHP single crystals at cryogenic temperatures, the exciton absorption resonances are significantly broadened and cannot be accurately resolved. Thus, E_b is often determined by:

$$E_b = E_g - E_{res} \quad (3)$$

where E_{res} is the 1s exciton resonance energy. In traditional optical spectroscopy experiments, surface artifacts, photo reabsorption, and microstructure in MHP thin films contribute to spectral broadening and the appearance of several peak shoulders that further complicate the determination of the E_g and E_{res} energies.[37] Given the challenges associated with determining E_g and E_{res}, E_b is often wrongfully assigned in MHPs. A case in point is the significant disparity in the experimental E_b value reported in the literature for $MAPbI_3$, which has sparked a heated debate in the photovoltaics community as to whether charge carriers in MHP are primarily bound electron-hole pairs or free electrons (or holes) at room temperature.[4,10,12,39-42] Many researchers have explored this open-ended uncertainty using traditional steady-state absorption spectroscopy and have determined that the E_b values range from 5-30 meV at room temperature.[18,43] The optical methods used to determine E_b values rely on gathering indirect results obtained from inadequate fitting procedures which assume homogenous linewidth broadening of a Gaussian exciton peak in the absorption spectra.[44] An alternative method, such as magneto-absorption, provides consistent and reproducible results only at cryogenic temperatures. This is because magneto-absorption does not have the resolution needed to distinguish between band-to-band transitions and exciton interactions at room temperature.[36,37,45] Furthermore, magneto-absorption relies on a hydrogenic model (equation 2) which should be treated as an approximation for MHPs. In contrast, EA spectroscopy can provide sensitive and sharp spectral features at critical points in the density of states that allow for model-independent determination of E_g and E_{res}.[46] For example, in $MAPbI_3$, the sensitivity of the EA line shape to the curvature of the dielectric function allowed for a measurement of E_b = 7.4 meV at room temperature.[10] Given that the separation between E_g and E_{res} is less than the thermal energy k_BT ~ 25 meV at room temperature, it is understandable that traditional spectroscopies would fail to obtain an accurate measurement. This small binding energy is one of the fundamental attributes of $MAPbI_3$ that allows it to perform so well when incorporated into photovoltaic devices compared to other solution-processed semiconductors such as organic semiconductors or inorganic quantum dots.

EA spectroscopy: working principles

In an EA experiment, the absorber layer within a thin film device is subjected to an externally applied AC voltage. The voltage can be applied in a lateral or perpendicular orientation with respect to the substrate. Because the applied voltage per unit area required to modulate the dielectric function (ε) can be tens of kilovolts per square centimeter, factors such as Joule heating must be taken into account to avoid sample degradation. To minimize thermal effects due to Joule heating, various EA studies have resorted to the use of patterned interdigitated electrodes where the distance between electrodes can be modified on the order of tens of microns.[19,47,48]

EA spectroscopy measures the change in absorption (ΔA) in the presence of an applied external field as per the following equation:

$$\Delta A(E) = A_{field}(E) - A_{no\ field}(E) \quad (4)$$

where E is the photon energy and $A(E)$ is defined as:

$$A(E) = -log_{10}(T(E)) \quad (5)$$

where $T(E)$ is the transmittance. From a physical point of view, when an electric field is applied to a material, the charge densities and dipoles within the material shift and reorient, hence modifying the nuclear configuration and ultimately the electronic structure. Solving for the field-induced energy shifts of the absorbing states is clearly outside the scope of analytical solutions, and therefore, the analysis of the EA spectra is divided into two broad categories of approximations based on the type of absorbing state that is being modulated, i.e., bound or unbound states, as discussed below.

Bound states

When an electronic state's binding energy is much greater than the perturbation of the applied field, as is the case for tightly-bound

excitons or molecular orbitals, a perturbation theory approach is valid. In such cases, the small change in energy (ΔE) caused by the applied electric field is determined by the relative change in polarizability ($\Delta\alpha$) and dipole moment ($\Delta\mu$) for an electronic transition from the ground state to an excited state. Modulation of a tightly-bound state results in linear and quadratic Stark shifts proportional to $\Delta\mu$ and $\Delta\alpha$, respectively, as described by Stark theory:

$$\Delta E \propto -\Delta\mu F - \frac{1}{2}\Delta\alpha F^2 \qquad (6)$$

where F is the applied electric field.[49-51] The change in transition dipole moment (Δμ) can be thought of as the amount of charge-transfer associated with an optical transition, whereas the polarizability represents the transition's sensitivity to an applied field. Assuming the states are tightly bound, the applied field can be treated as a small perturbation and the EA signal (ΔA) can be approximated by a Taylor-series expansion around a small ΔE:[14,52]

$$\Delta A = -\frac{\partial A}{\partial E}\Delta\mu F - \frac{1}{2}\frac{\partial A}{\partial E}\Delta\alpha F^2 + \frac{1}{2}\frac{\partial^2 A}{\partial E^2}(\Delta\mu F)^2 \qquad (7)$$

In an isotropic material, the transition dipole moments are randomly oriented and therefore the first term, which is dependent on the field direction, averages to zero. Thus, the experimentally observed EA spectrum scale in amplitude according to the applied field square (F^2) and resemble first and second derivatives of the absorption spectrum.

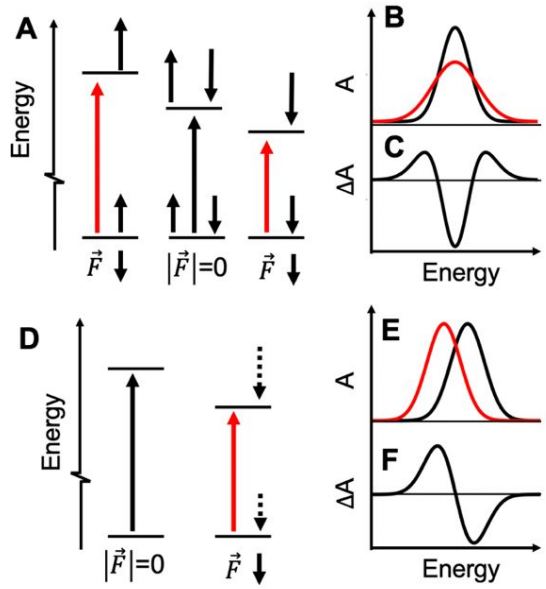

Figure 3. (A) Interaction of an applied electric field with two different orientations aligned with and against the field. **(B)** Corresponding band broadening and **(C)** resulting change in absorption. **(D)** Interaction of an applied electric field on a transition that has a change in polarizability. **(E)** Peak with (red) and without (black) an applied electric field. **(F)** Resulting EA spectrum due to a change in polarizability.

Analysis of the EA line shape allows one to interpret the fundamental characteristics of the bound electronic states that are being modulated by the electric field. Bublitz and Boxer described the relationships between the first and second derivatives of the absorption and EA spectra for tightly bound charges through the Stark effect as illustrated in **Figure 3**.[49] These relationships were initially derived for molecular systems, such as donor/acceptor π-conjugated systems, but can be applied to any system with discrete absorption bands.[14,53,54] In a system with randomly oriented electric dipole moments (μ) with respect to the applied electric field (F), the absorption of that transition is broadened. For example, if a sample contains two different orientational subpopulations, the electronic transitions will be shifted differently depending on their dipole direction (**Figure 3A**). In the presence of an electric field, the subpopulations will shift to higher or lower energies. An ensemble of randomly distributed transition dipole moments will therefore broaden the absorption (**Figure 3B**) and the EA spectrum correspondingly resembles the second derivate of absorption (**Figure 3C**). Examples of absorption features with large Δμ values are molecular states with large dipole moments, charge-transfer excitons, and excitons with asymmetric charge density due to morphological disorder such as defects or amorphous grains.[55] Conversely, a field-induced dipole due to a state's polarizability ($\Delta\alpha$) is always aligned with the applied field, as shown in **Figure 3D**. Therefore, rather than broadening the absorption, the difference in polarizability between the two states, $\Delta\alpha$, uniformly redshifts the absorption to a lower energy according to the quadratic Stark effect (**Figure 3E**) resulting in a first derivative line shape, as shown in **Figure 3F**. Examples of systems that experience a quadratic Stark effect are polarizable molecules and Wannier excitons. A Stark shift of the latter is formally analogous to the hydrogen atom's Stark shift and is one of the few systems for which EA spectrum has been solved theoretically.[56]

The EA response of a bound state includes another phenomenon worthy of mention that is not accounted for by **equation (7)**, that is field ionization. When an applied field ionizes a bound state, the state's lifetime decreases and its spectra correspondingly broadens according to the time-energy uncertainty principle. Fortunately, a second derivative line shape due to field-ionization can usually be distinguished from one caused by a large Δμ with careful consideration of the absorption band in question. First, broadening due to field ionization of a bound state below a continuum (such as an exciton) will be asymmetric, as the state will favor ionization into the conduction band.[57] Second, the likelihood of observing field ionization can be readily determined by comparing the applied field strength to the binding energy of the state in question. In the case of an exciton, this is most aptly done by calculating the ionization field (F_I), or the field required to create a potential drop of 1 E_B across the exciton's radius (a_B):

$$F_I = E_B/|e|a_B \qquad (8)$$

The value of F_I is on the order of ~ 10^6 V/cm for 3D MHPs,[10] but is on the order ~ 10^8 V/cm for 2D MHPs. Since experimental fields are typically on the order of 10^6 V/cm, a contribution of spectral broadening due to field ionization is expected in 3D MHPs, but far less likely in 2D MHPs.

Lastly, when considering low-dimensional systems such as multiple quantum wells or quantum dots, there is another relevant effect that must be considered when the field is applied in the direction of quantum confinement, namely, the quantum-confined Stark effect (QCSE). Similar to the quadratic stark effect, the shift in energy due to the QCSE is negative and scales with the field strength squared. As a result, the exciton resonance redshifts and the EA line

shape has a first derivative shape that scales quadratically with field strength.

At the conduction band-edge, however, the continuum states are not bounded and a fundamentally different approach is needed to understand these spectral features.

Unbound states

For unbound states, the EA signal response is described by the Franz Keldysh (FK) effect.[15,17,19,58] In brief, due to the fact that unbound continuum states are free to accelerate along field lines, the Bloch states turn to Airy states. The EA spectrum oscillates according to an Airy function with an argument that is the electron's kinetic energy $E - E_g$ normalized by an electro-optic energy, $\hbar\theta$, as follows:

$$\Delta A \propto Ai\left(\frac{E-E_g}{\hbar\theta}\right) \quad (9)$$

$$(\hbar\theta)^3 = \frac{(e\hbar F)^2}{2\mu} \quad (10)$$

where E is the photon energy, E_g is the bandgap, μ is the reduced mass at the band-edge.[10,59-61] While the EA spectrum should resemble a derivative-like line shape in the exciton region, the spectrum oscillates according to the form of the Airy function above the band edge where electrons are excited into the conduction band continuum, as depicted in **Figure 4A-B**. Exactly at the band-edge the Airy state leaks into the forbidden gap, creating a unique interband oscillatory period that smoothly transitions into the FK oscillations. These above-gap FK oscillations broaden proportional to $\hbar\theta \propto F^{2/3}$ and increase in amplitude proportional to $\sqrt{\hbar\theta} \propto F^{1/3}$. This field-dependent behavior makes such features easily discernible from the Stark-shifted exciton states below the bandgap, which exhibit field-invariant line shapes and amplitudes that scale quadratically with $\propto F^2$. Herein lies the effectiveness and the scientific beauty of EA spectroscopy. By a simple determination of the power-relation between EA amplitude and applied field strength, EA spectroscopy can be easily used to distinguish between bound and unbound states.

In traditional low defect semiconductors, such as GaAs, clear FK oscillations have been resolved for multiple oscillatory periods spanning a wide spectral range of ~ 0.5 eV.[62] However, observing FK oscillations in MHPs has been proven to be challenging.[10,12,63] Various factors affect FK oscillations, such as energy-dependent broadening effects, surface effects, non-uniform modulation, non-flatband modulation, photovoltage effect, and Coulomb effects.[59] Heesel *et al.* demonstrated that electron-hole Coulomb interactions in GaAs, even at fields as high as 30 kV/cm, can decrease the amplitude of FK oscillations by a factor of 2.[64] Therefore, it is not surprising that FK features are weak in the highly ionic MHPs lattice wherein electron-phonon scattering events frequently occur.[65,66] These scattering events disrupt the wavefunction coherence required to distinguish multiple FK oscillations; hence, experimentally, only the first oscillation is typically observed.[67-71] The contribution of the FK effect to the EA signals remains a topic of open debate. We believe the debate could be easily addressed if there were more efforts devoted to developing theoretical models that could help describe convoluted FK oscillation features in MHPs.

The EA response above the bandgap has a different behavior when the perturbation of the applied field is much smaller than the material's homogenous broadening function, Γ. In the low-field limit, when $\hbar\theta < \frac{1}{3}\Gamma$, the EA signal relates to changes in the complex dielectric function ($\Delta\varepsilon$) through a proportionality constant called the Seraphin coefficient (a), as follows:

$$\Delta A \approx a\Delta\varepsilon \quad (11)$$

Furthermore, in such a low-field regime, $\Delta\varepsilon$(E) (and therefore the EA signal) simplifies to a third-derivative line shape of the complex dielectric function ε(E) as follows:[59,72,73]

$$\Delta\varepsilon(E,F) = \frac{(\hbar\theta)^3}{3E^2}\frac{d^3}{dE^3}\left(E^2\varepsilon(E)\right) \quad (12)$$

where E is the photon energy and F is the applied field. Combining (11) and (12), it becomes clear that EA and ellipsometry are powerful complimentary techniques for the low-field regime. Ellipsometry provides the complex dielectric function ε(E) which can then be fit to the EA signal to obtain $\hbar\theta$. Further modelling can yield accurate measurements of the exciton binding energy that would otherwise be inaccessible due to the material's large broadening function and overlapping spectral features.[10]

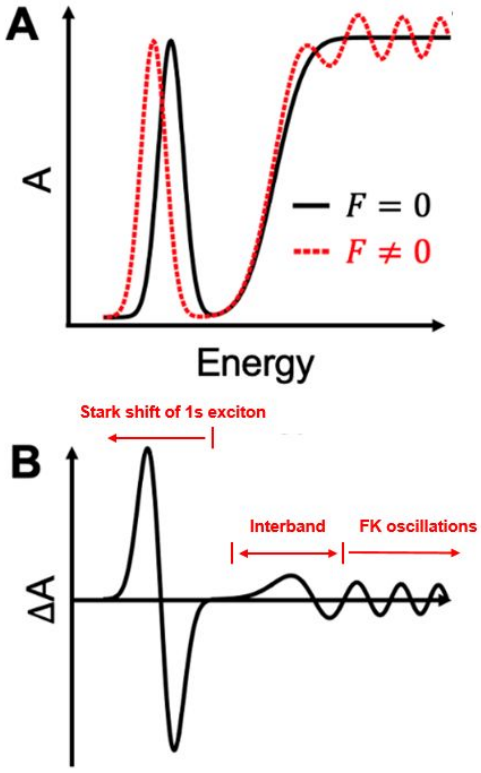

Figure 4. (A) Cartoon representation of the effect an applied field has on bound states, such as excitons below the bandgap which are governed by the Stark effect, or unbound continuum states above the bandgap, governed by FK oscillations. Exactly at the band edge, the continuum wavefunction leaks into the gap, creating an interband feature in the EA spectrum. **(B)** The resulting difference (EA) spectrum. When overlapping exciton states and continuum states are present, it can be useful to plot the amplitude of the EA signal vs F^{γ} to help differentiate mixed optoelectronic states. As discussed, excitons scale linearly to $\gamma = 2$, whereas continuum states scale linearly to $\gamma = 1/3$.

In summary, a quick visual inspection of the line shape of the EA spectra, when compared to the numerical derivative, can provide

insight into the optoelectronic characteristics of the carriers affected by the electric field. There are usually two observed features for MHPs possessing excitons with high binding energy and continuum states in quantum well-like crystal lattices: a Stark shift of the exciton below the bandgap and an FK-type oscillation at the band-edge.[74] In confined, low dimensional MHPs, the first derivative-like line shape is often typical of 1s excitons with large binding energies whose ionization fields are much larger than the applied electric field.[15,17,19,58] Changes in polarizability ($\Delta\alpha$) can be interpreted as an electron distribution response to an externally applied electric field.[75] When charge carriers or excitons are polarizable Wannier excitons, as they are in 2D layered MHPs, the $\Delta\alpha$ is large and a first derivative EA line shape is expected. Second derivative line shapes corresponding to a large transition dipole moment ($\Delta\mu$) are expected if the bound state is a charge-transfer exciton, has a disorder-induce dipole moment, or is significantly ionized. Finally, third derivative line shapes and coherent oscillations are both descriptors that the excited state is a delocalized continuum.[17,47,76] Critical points in the absorption spectrum (such as exciton or bandgap transitions) can be difficult to deconvolute when they overlap. In EA spectroscopy, these features cause unique derivative-like curves in the modulated EA spectrum, therefore allowing for their separation and characterization.

Critical points

EA spectroscopy has the advantage of providing extremely sharp spectral signatures related to localized and delocalized states due to the elimination of optical scattering and background absorption from broad neighboring critical points.[10,36,46] Critical points (also known as Van Hove singularities) are singularities in the density of states. They are observed physically in the absorption spectrum as features such as exciton or bandgap transitions.[77] Analyzing MHPs using optical techniques such as ellipsometry or reflection spectroscopy are known to be detrimentally affected by scattering and background absorption; therefore, they require complex surface state analysis to accurately interpret the data.[78-81] For example, given that in $MAPbI_3$, the exciton binding energy is reported to be less than thermal energy; therefore, the exciton and bandgap will have considerable spectral overlap. This means that a discrete excitonic peak cannot be resolved, even at low temperatures.[82] In EA spectroscopy, the exciton peak's discrete location is either at the zero crossings, for the first and second derivative features, or at the peak, for the third derivative features. The relationship of localized carriers (i.e., excitons) vs. delocalized carriers (i.e., free carriers in the continuum) behave differently when subjected to an electric field. Even when the bandgap and exciton features spectrally overlap closely in steady-state absorption spectroscopy, they can be easily distinguished using EA spectroscopy. This makes EA spectroscopy a superior technique for determining the near-edge optical properties of semiconductors.[83,84]

Case studies

The following sections discuss key studies chosen to highlight the breadth of unique characterization available when coupling EA spectroscopy with traditional steady-state optical tools to investigate complex optical features in MHPs.

Comprehensive optical characterization of 2D layered MHPs

Low dimensional MHPs consist of naturally forming quantum wells that have alternating organic and inorganic sheets. Given the strong quantum confinement of charge carries arising from the dielectric constant mismatch between the alternating organic and inorganic layers, MHP quantum well heterostructures exhibit unique optoelectronic properties such as large exciton binding energies (>100 meV), tunable bandgaps, strong spin-orbit coupling, and giant Rashba splitting close to the extrema in the valence and conduction bands.[47,85-88] Through a combination of photoinduced absorption, EA spectroscopy, and theoretical studies, Zhai *et al*., were able to extract delicate absorption features from a broad absorption background using the modulated EA spectrum for phenethylammonium lead iodide [$(C_6H_5C_2H_4NH_3)_2PbI_4$; also known as PEPI] thin films. **Figure 5A** depicts the crystal structure for PEPI. Here, the organic ($C_6H_5C_2H_4NH_3^+$) and inorganic $[PbI_6]^{4-}$ layers naturally arrange to form a 2D layered structure comprising multiple quantum wells with a thickness of ≈ 1 nm (organic layer, also known as the barrier) and ≈ 0.6 nm (inorganic layer, also known as the well), respectively. **Figure 5B** shows that the photoluminescence (PL) and absorption features in PEPI are dominated by a strong exciton peak around 2.4 eV. The absorption spectrum has an additional broad onset feature that slowly rises, starting around 2.6 eV, which appears to be related to the bandgap. However, it is challenging to precisely identify the bandgap energy and assign the origin of buried features from this absorption plot. There is no sharp absorption onset that a Tauc plot can be applied to, and again, the results would vary significantly depending on the region chosen in the linear regression.

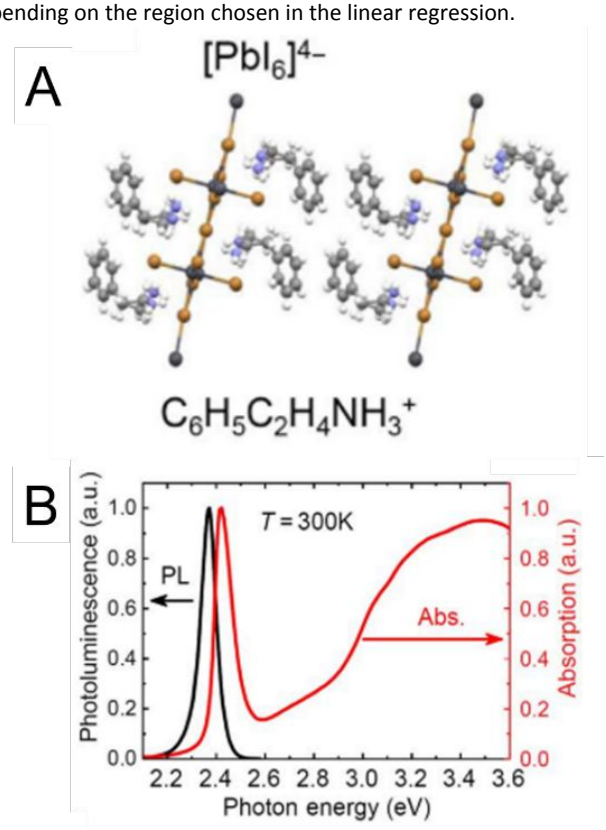

Figure 5. (A) Crystal structure, **(B)** room temperature optical absorption (red) and photoluminescence emission spectra (black) for PEPI thin films. Reproduced with permission from *Sci. Adv*. 2017, 3 (7), e1700704 (ref 19). Copyright 2017 Science Advances.[19]

As validated by the studies performed by Zhai *et al*., EA spectroscopy studies were proven to be a viable route for elucidating the precise nature of the optical properties of PEPI.[19] The temperature-dependent absorption and low-temperature (10 K) electroabsorption spectra are presented in **Figure 6A-B**. Even at low temperatures, where absorption features often sharpen, there is insufficient information in the absorption spectra to confidently

assign the different exciton absorption transitions (**Figure 6A**). When comparing the absorption data to the EA data, the forte of the latter technique is easily realized. As depicted in **Figure 6B**, the EA spectrum is divided into two distinct regions, i.e., excitonic features behaving in accordance with the Stark effect and band-edge features following the FK effect.[47,74,89] The 1s exciton is strongly perturbed within the electric field, showing a first derivative-like curve that crosses zero at 2.38 eV. This is consistent with a Stark shift of a highly localized state, resulting in a redshift in the presence of an applied electric field. From the absorption studies, the broad step-like feature near 2.6 eV may be assigned as the E_g for PEPI. However, this may be improperly assigned given that differentiating between the 2s exciton and the E_g is nearly impossible when using conventional absorption characterization tools. In the EA spectrum, the 2s and E_g are differentiated critical points, but separating exciton vs. continuum states requires the electric-field dependence to be properly established. Furthermore, as stated previously, the Stark effect scales quadratically with the applied electric field in the form of voltage (V). By comparing the EA amplitude to V^2, Zhai *et al.* were able to differentiate excitonic and continuum features (**Figure 6C-E**). The EA amplitudes at 2.36 eV, 2.40 eV, and 2.48 eV were all plotted against V^2. Here, a linear relationship is shown, indicating the modulation of localized states that can be assigned to excitons.

Evidence of FK oscillations in MHPs is not common because these oscillations are dampened by crystal defects, grain boundaries, and other non-uniformities.[59] However, some 2D MHPs self-assemble into highly-oriented quantum well structures that, due to their anisotropic nature, their EA profile shows clear evidence for the existence of FK oscillations with a sufficiently high applied electric field. As previously discussed, FK oscillations are observed experimentally in EA spectroscopy when the –ΔT/T vs photon energy curves as a function of increasing applied voltage do not converge at zero. Instead, the EA features broaden with increasing voltage and the zero-crossing points split apart in energy, highlighted in **Figure 7A** near the labeled point "c". This is in stark contrast to the 1s exciton derivative feature where all voltages share a common zero-crossing. In **Figure 7B**, the labeled point "c" represents the multiple zero crossings and "d" the blueshift that increases with the applied electric field. Zhai *et al.* confirmed that these features are not derived from the Stark effect by plotting the amplitude vs. V^2, shown in the inset, where there is an apparent deviation from the linear relationship at high applied field strengths.

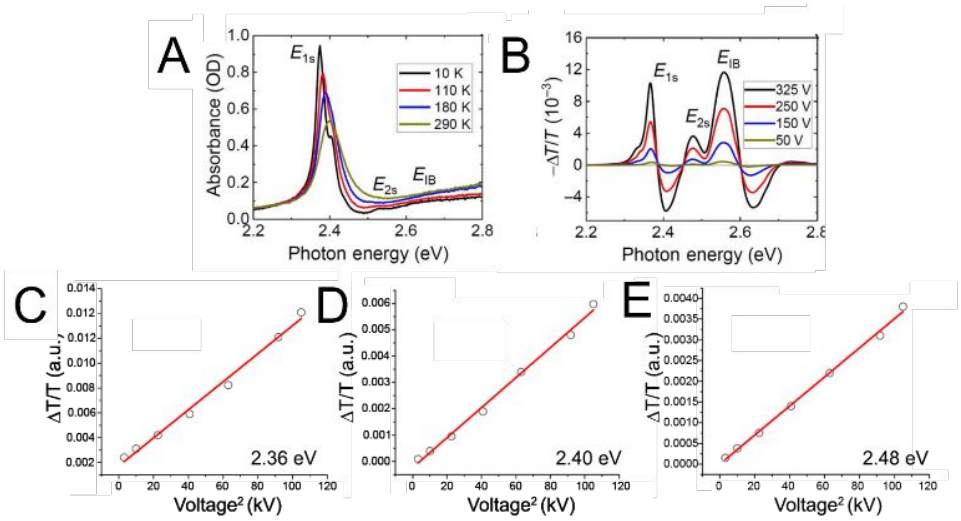

Figure 6. (A) Temperature-dependent absorption for PEPI thin films. **(B)** EA spectra measured at 45 K at field strengths ranging from 50 to 325 V. **(C-E)** V^2 dependence of EA amplitude of features below the interband transition edge. Reproduced with permission from *Sci. Adv*. 2017, 3 (7), e1700704 (ref 19). Copyright 2017 Science Advances.[19]

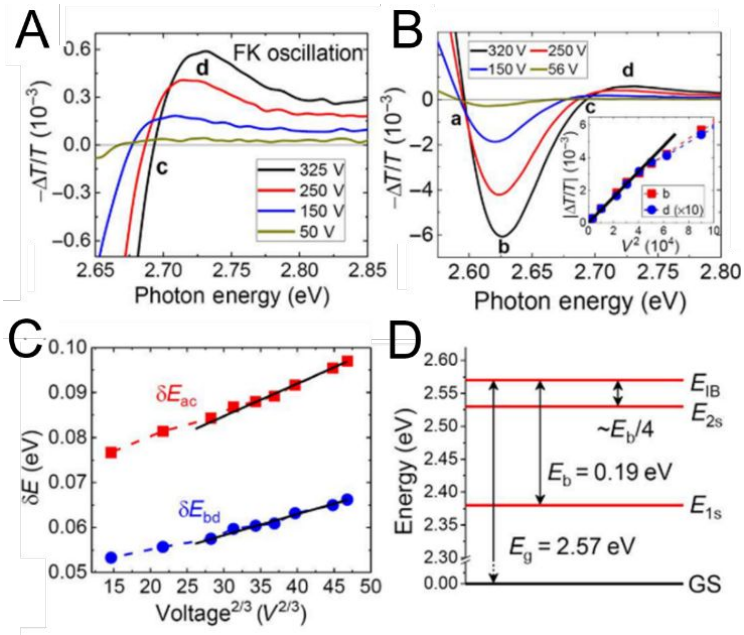

Figure 7. (A) EA spectra for PEPI thin films highlighting the Franz Keldysh (FK) oscillations. "c" represents the zero crossing; "d" denotes the blueshift caused by the oscillations. **(B)** Highlighted regions centered around 2.65 eV. "a", "b"," c" and "d" represent the zero-crossing energies and peak positions, respectively. Inset shows V^2 dependence of exciton features that saturate at high voltage. **(C)** Energy differences showing $V^{2/3}$ dependence. **(D)** Energy levels of the excitons (E_{1s} and E_{2s}), bandgap (E_g), interband transition, and binding energy (E_b). Reproduced with permission from *Sci. Adv*. 2017, 3 (7), e1700704 (ref 19). Copyright 2017 Science Advances.[19]

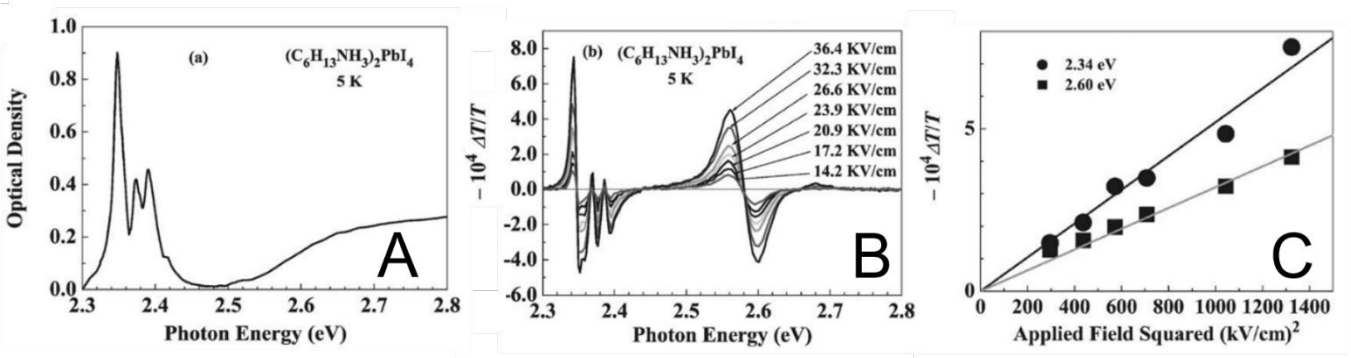

Figure 8. (A) Absorption spectrum of $(C_6H_{13}NH_3)_2PbI_4$ thin films. **(B)** Electroabsorption spectrum under applied fields ranging from 14.2 kV/cm to 36.4 kV/cm. **(C)** Linear relationship between the amplitude of EA peaks and the applied field squared. Reproduced with permission from *Solid State Commun.* 2002, *122*, 249-252 (ref 15). Copyright 2002 Elsevier.[15]

To test if the features around 2.7 eV are from the bandgap modulation, both zero crossings (ΔE_{ac}) and peak location (ΔE_{bd}) were plotted against $F^{2/3}$ (**Figure 7C**). The resulting linear relationship confirms that this feature lies above the band edge; therefore, the oscillatory period which precedes it was assigned as an interband feature associated with the continuum wave-function leaking into the forbidden gap. Pinpointing the exact bandgap energy within this interband oscillatory period requires careful consideration of the system in question and often requires modelling. In accordance with FK theory on 3D direct-gap semiconductors, Zhai et al decided to assign the first peak of the IB feature as E_g.[72] Thus, from the EA spectrum for PEPI at 50K, Zhai *et al.* were able to assign E_g, 1s, and 2s excitons and their respective binding energies, resulting in the schematic depiction of a full electronic energy level diagram (**Figure 7D**). A recent study by Hansen *et al.* analyzed the EA spectrum of the same material, but complemented the measurement with sophisticated modelling of a 2D Wannier exciton in a uniform electric field (or the high-field Franz-Keldysh effect).[90] By doing so, the authors were able to pinpoint the bandgap energy with high confidence within the IB feature and improve upon Zhai *et al.*'s measurement, resulting in an extremely precise exciton binding energy measurement of 223 ± 3 meV for PEPI.[90] Thus, it is clear that the interpretation of some EA features, such as exciton Stark shifts in this case, are more straightforward than others such as the IB feature. In some instances, modelling the EA signal according to low- or high-field Franz-Keldysh effects is necessary for quantitative analysis of the EA spectrum as the IB feature could be mistaken as the ionization of the 2s exciton state.

Derivative line shape analysis

Tanaka *et al.* investigated the optical features of a similar 2D MHP material, namely hexylammonium lead iodide ($(C_6H_{13}NH_3)_2PbI_4$) via EA spectroscopy. The authors used derivative line shape analysis to show the multiple discrete peaks below the band edge arise from a quadratic Stark shift of the 1s exciton and its corresponding phonon sidebands. **Figure 8** depicts the absorption and EA spectra acquired at 5K. By analyzing the absorption data in **Figure 8A**, the 1s exciton resonance can be clearly assigned at 2.34 eV with associated phonon sidebands around 2.40 eV. However, from this data, it is not clear where the band gap energy is within the broad step-like feature. From the EA spectra provided in **Figure 8B**, Tanaka *et al.* acquire considerably more information about the optical features for the 2D MHP system, particularly at higher energies. In the EA spectrum, a large interband feature appears around 2.60 eV, associated with wavefunction leaking into the forbidden gap. By plotting the EA features' amplitude at 2.34 eV and 2.60 eV, they observe both the exciton and the interband features have quadratic dependence with applied field (**Figure 8C**).

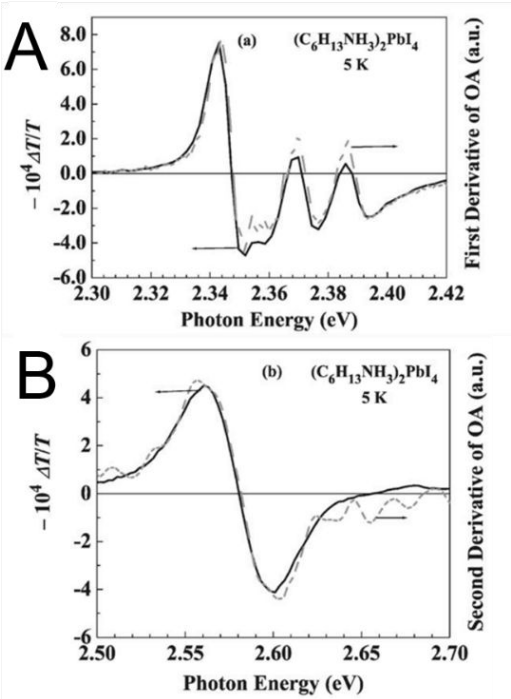

Figure 9. (A) EA spectrum (solid line) and first derivative of absorption (dashed line) of the 1s exciton and its phonon sidebands. **(B)** EA spectrum (solid line) and second derivative of bandgap's step-like absorption (dashed line) which coincidentally has the same functional form as the interband EA feature. Reproduced with permission from *Solid State Commun.* 2002, *122*, 249-252 (ref 15). Copyright 2002 Elsevier.[15]

By performing the line shape analysis, Tanaka *et al*. show a near-identical match between the EA spectrum and the first derivative of the absorption spectrum in the excitonic region as shown in **Figure 9A**. Provided instrumental corrections are accounted for, the scalar relationship between these two spectra can used to measure the exciton's polarizability according to equation 7. Indeed, it was this strong first derivative response that first alerted researchers to the highly polarizable Wannier-exciton nature of excited states in 2D MHPs. In another complimentary study, Tanaka et al compared this in-plane EA spectrum to its out-of-plane counterpart, i.e., with an applied field perpendicular to the quantum well layers.[17] The anisotropy between the two directions was the first clear demonstration of the excited state's two-dimensional character, highlighting the historical importance of EA in elucidating the fundamental nature of excited states in 2D MHPs and other multiple-quantum well systems.[91,92] As shown in **Figure 9B**, the second derivative of the bandgap's step-like absorption is coincidentally the same line shape as the interband feature. However, to evaluate this portion of the spectrum according to equation 7 for bound states would be incorrect since the absorbing state is an unbound continuum in the conduction band. This example highlights the importance of using absorption and EA as complementary techniques. Knowing that the step-like absorption feature corresponds to an unbound band-to-band transition helps one avoid an incorrect assignment of the second derivative feature to a broadened bound state.

Investigating ion migration in MHPs upon perturbation of the internal electric field

EA experiments are conducted by applying an AC voltage to an MHP thin film. If there is an internal field due to a change in charged ion distribution in a sample, this will be seen as a reduction in the EA amplitude. This is because the quadratic Stark shift relates the local electrostatic field in the MPH layer to the quadratic field dependence (F^2).[93] Therefore, the square root of the EA signal can provide a direct measurement of the electrostatic field and be used to monitor any buried optical changes. Kim *et al*. cleverly leveraged this relationship to understand the ion migration properties of $MAPbI_3$:BAI (BAI = butylammonium iodide) thin films as potential active layers for LED applications.[7]

Investigating ion migration effects in their samples was spurred by their findings that at low current densities (>10 A cm^{-2}), the external quantum efficiency (EQE) had a strong dependence on the time of the pulsed optical bias; however, in DC (non-pulsed) operation, their EQE was significantly lower. They proposed that this behavior was linked to ion migration within the MHP layer because I^- drift occurs on time scales of milliseconds to seconds.[94,95] If ion migration occurs, then the internal electric field would change due to charge redistribution. When the authors increased the optical pulse duration, the EQE ideality factor (η) dropped from η ≈ 2.2 to η ≈ 1.6. The η value provides insight into the type of recombination that is occurring within the diode architecture. This difference suggests that the diode shifts from being dominated by trap-mediated recombination to a more radiative bimolecular recombination, which would be linked to ion migration.

To determine if there were an internal electric field change due to ion migration, Kim *et al.* performed static and time-dependent EA studies on $MAPbI_3$:BAI thin films. As depicted in **Figure 10A**, the EA signal of the $MAPbI_3$:BAI diode is used as an indicator of the external electric field. In **Figure 10B**, the time-dependent EA signal (at 730 nm) in response to a 10 ms voltage pulse mirrors the applied voltage, concluding that ion migration is not occurring on that time scale. However, the response changes drastically when the applied voltage time is increased to 2 s (**Figure 10C**). The EA signal decays strongly, indicating that the applied field is internally screened on a 0.5 s time scale due to ion movement within the $MAPbI_3$ layer. Ion migration in MHPs has been both detrimental, causing large hysteresis effects in photovoltaic devices,[96] and advantageous, opening the possibility for memory devices based on ion motion.[97,98]

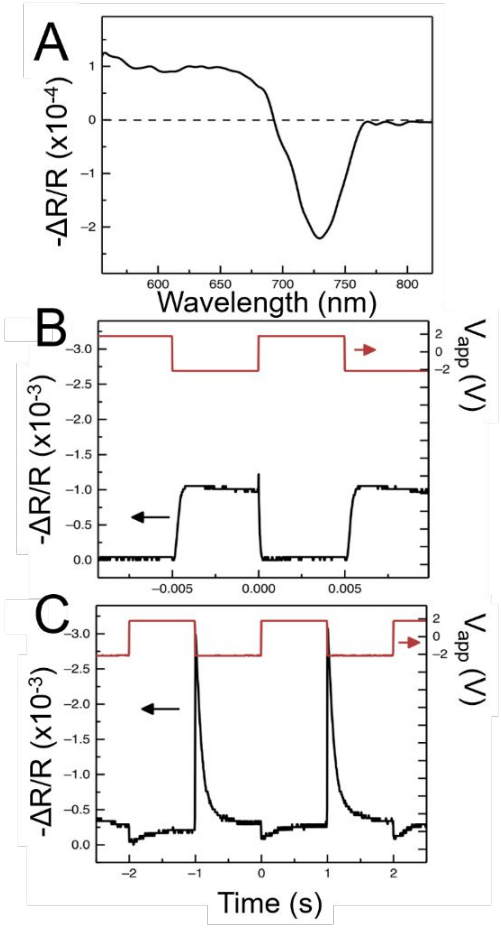

Figure 10. (A) EA of a device based on a $MAPbI_3$:BAI thin film in a reverse bias of -2 V with a 0.8 V dither at 389 Hz. **(B)** Transient EA response resulting from a 10 ms period square wave signal oscillating between +2V and -2V. **(C)** Transient EA response resulting from a 2 s period square wave signal oscillating between +2V and -2V. Reproduced with permissions from *Nat. Commun.* **2018,** *9*, 4893 (ref. 7). Copyright Springer Nature 2018.[7]

Quantifying phase heterogeneities in low dimensional MHPs

EA spectroscopy can be used to deconvolute intra-material optical properties, such as phase heterogeneities of MHP quantum wells. Ruddlesden-Popper (RP) phase metal halide quantum wells have the generic formula $A_{n-1}B_nX_{3n+1}$, where A' is a bulky spacer cation that serves as the barrier layer, A is an organic cation that serves as the well layer, B is a metal center, and X is a halide. By increasing or decreasing the quantum well thickness (*n*), the optical properties of the material can be tuned from a wide bandgap (n = 1, $E_g \approx 2.3$ eV) to a low bandgap (n = 5+, $E_g \approx 1.7$ eV) material, respectively. RP MHPs form a distribution of quantum well thicknesses (*n*) when cast into thin films, rather than creating pure-phase materials dictated by the stoichiometric ratios of the precursor solution.[99-102] The quantum well thickness only differs by a few angstroms; therefore, their respective optical properties, such as exciton resonance energy, are only separated by a few hundred meV. This results in a very complex and convoluted absorption profile that makes it difficult to pinpoint the optical properties of each *n.* The convolution of exciton resonance is observed in the absorption spectra depicted in **Figure 11**. For example, $(BA)_2(MA)_2Pb_3I_{10}$ (blue line) has absorption peaks from both the *n* = 2 and *n* = 3 exciton resonances. Still, due to the close energy spacing of these features, it is challenging to accurately determine the energy just from the absorption data.

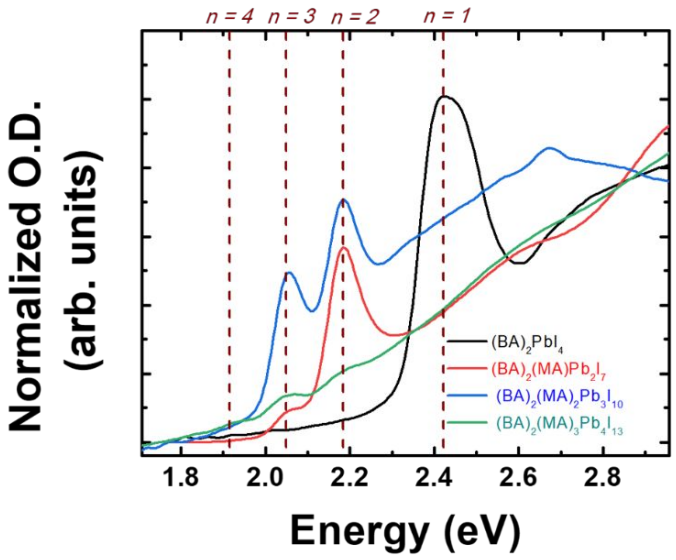

Figure 11. Optical absorption of $(BA)_2(MA)_{n-1}Pb_nI_{3n+1}$ for different quantum layer thicknesses (n = 1 - 4). Dashed lines indicate the exciton absorption resonances. Reproduced with permission from *ACS Appl. Mater. Interfaces* 2020, 12, 47, 52538–52548 (ref. 86). Copyright 2020 American Chemical Society.[86]

To elucidate the phase heterogeneity, Amerling *et al.* performed low-temperature EA studies on $(BA)_2(MA)_{n-1}Pb_nI_{3n+1}$ quantum wells (*n* = 1-4) and $MAPbI_3$ thin films, as shown in **Figure 12A**.[88] It is clear from the observed EA features that the samples are comprised of multiple excitons related to different quantum well thicknesses present within the thin film. The authors quantified the phase heterogeneity by investigating changes to the localized exciton absorption states as a function of quantum well thicknesses. The EA data were fit using a linear combination of the zeroth, first, and second derivative of the unmodulated absorption spectrum (equation 7). In brief, they determined the precise exciton resonance energies through the EA spectra utilizing the derivative-like shapes that result from this experiment. Using the precise exciton resonance energies, a Gaussian function was used to model the exciton peaks with an additional polynomial function to account for band-to-band absorption. Finally, they scaled the Gaussian amplitudes by the relative oscillator strengths of the different types of excitons present; this is particularly important when dealing with MHPs because of the well-known strong absorption cross-sections; therefore, the oscillator strengths play a crucial role in the absorption intensities.[103] The heterogeneity of the quantum well distribution was then determined by analyzing the relative amplitudes of the exciton Gaussians that were used to fit the EA and absorption data. The fitting routine is visualized in **Figure 12B**.

The final quantification of the phase heterogeneity is shown in **Figure 12C**. We can see that the intended phase pure quantum well distribution varies significantly from the resulting distribution determined post-synthesis. This was attributed to an interplay between kinetic and thermodynamic stabilities inherent to the stoichiometry of the quantum well for the MHPs. As such, EA is a technique that is sensitive to small changes in the absorption spectra of heterogeneously dispersed quantum wells within a single thin film. The analytical approach developed by Amerling *et al.* uses a

combination of EA and absorption spectroscopies as a way to precisely determine the exciton resonance energies and uses those energies to build a model that fits the absorption spectra to quantify the quantum well thickness distribution throughout a given thin film. The enhanced understanding of these MHP thin films allows for tailored heterostructures that rely on precise control over the phase distribution. This work is also an example of how researchers can identify and quantify the exciton heterogeneity (and hence structural heterogeneities) of many different heterogeneous materials, such as core-shell quantum dots or bulk heterojunction organic semiconductor materials.

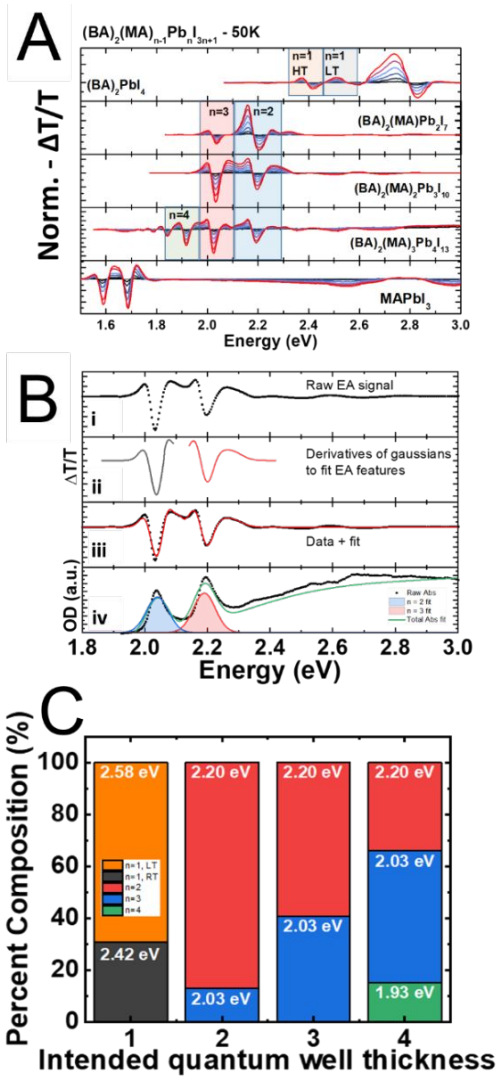

Figure 12. (A) EA spectra of $(BA)_2(MA)_{n-1}Pb_nI_{3n+1}$ (n = 1 - 4) and 3D $MAPbI_3$ measured at 50K. **(B)** Example of fitting routine used for investigating exciton compositions in $(BA)_2(MA)_{n-1}Pb_nI_{3n+1}$ quantum wells. Here the raw absorption data (i), the linear combination of the zeroth, first, and second derivatives of Gaussians to represent the EA curves (ii), the agreement of fits with experimental EA data (iii), and the resulting absorption exciton fits used to determine the quantum well heterogeneity (iv) are presented. **(C)** Pure phase quantum well distribution determined by the EA fitting parameters. Reproduced with permission from *ACS Appl. Mater. Interfaces 2020*, 12, 47, 52538–52548 (ref. 86). Copyright 2020 American Chemical Society.[86]

Distinguishing excitonic and band-to-band transitions in 3D MHPs

In low dimensional lattice and molecular systems, such as 2D layered MHPs, their EA spectra exhibit first or second derivative-like line shapes, which are attributed to the presence of bound excitons within the sample.[9,13,15,17] However, as described by the seminal work by Aspnes, the EA spectra for 3D MHPs such as $MAPbI_3$ resemble a third derivative-like line shape that is indicative of the presence of unbound electrons and holes in the crystalline lattice.[9,10,46] Nevertheless, there are still conflicting results in the literature when it comes to the expected line shape of the EA spectra for 3D MHPs. These conflicting results stem from whether charge carriers are bound or unbound in 3D MHPs and how that influences the first, second, or third derivative EA line shape.[8,104] The common ground between these conflicting results is that researchers struggle to consider the excitonic effects, no matter how small, when analyzing the EA spectra. To study excitonic effects in $MAPbI_3$, Ruf *et al.* performed temperature-dependent EA studies and measured the fundamental bandgap and exciton binding energy of $MAPbI_3$.[12] The absorption spectrum (black line, **Figure 13A**) shows the band-edge onset near 1.6 eV for a 3D $MAPbI_3$ thin film. The numerical first, second, and third derivatives were calculated to determine which line shape fit showed the strongest qualitative agreement with the EA signal. Since a phase shift in lock-in detection can reverse the sign of the EA signal, the first and third derivatives are qualitatively similar, and both resemble the EA signal. Moreover, the third derivative should model the EA signal most closely with the assumption that $MAPbI_3$ is a free carrier system. In contrast, an excitonic system would be expected to have a strong first derivative signal. Previous studies have analyzed the signal from opposing perspectives and have arrived at different measured E_b values.[10,12,16] As illustrated in **Figure 13A**, Ruf *et al.* focused on analyzing the EA signal for a $MAPbI_3$ thin film from the perspective of a first-derivative response. At 190 K, an exciton resonance is observed at the band-edge absorption. As evident from the EA spectra for 2D MHPs, the exciton and continuum responses differ significantly in nature. In 3D MHPs, the energetic separation between exciton and continuum states is far less, and the EA spectral features overlap. There is a compelling level of qualitative agreement in the line shapes of the EA and first derivative spectra, treating the combined exciton-bandgap features collectively as a first derivative shift, expected from the exciton's polarizability. However, it fails to account for spectral contributions from field-ionization and any portion of electrons that are excited into the continuum states.

In 2016, a study by Ziffer *et al.* modeled the EA spectrum of $MAPbI_3$ according to low-field Franz-Keyldsh theory, where the unperturbed complex deflection function was obtained via ellipsometry (**Figure 13B**).[10] First-principles calculations of a Wannier exciton in an electric field were also carried out to study the contribution of field-ionization. This field-ionization, or the ionization of a bound state, may result in a decrease in the carrier lifetime, which broadens the absorption and results in a second derivative line shape.[57] The validity of their approach was confirmed by accurate measurements of known values for E_b and E_g in GaAs. The careful analysis led to the precise determination of an $E_b = 7.4 \pm 1.2$ meV for $MAPbI_3$ thin films.

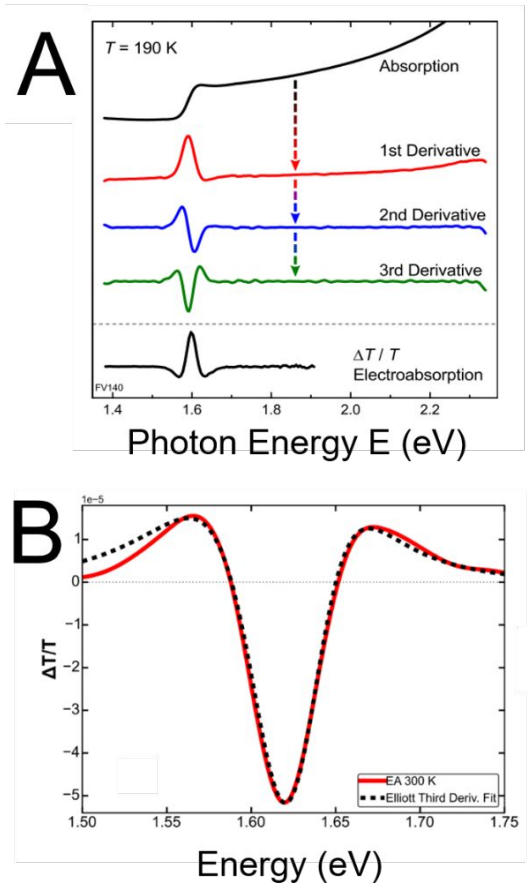

Figure 13. (A) Absorption spectrum and calculated first, second, and third derivative plots compared to the EA spectrum for $MAPbI_3$ thin films investigated by Ruf *et al.* **(B)** EA (red line) and third derivative fit (dashed line) for $MAPbI_3$ thin films studied by Ziffer *et al.* (A) Reprinted with permissions from *Appl. Phys. Lett*. 2018, 112, 083902 (ref. 12). Copyright 2018 AIP Publishing. (B) Reproduced with permissions from *ACS Photonics* 2016, *3*, 1060-1068 (ref. 10). Copyright American Chemical Society.[10,12]

Electroabsorption modulators based on quantum confined-Stark effects

In addition to elucidating the character of excited states, EA studies also have technological relevance in that each device functions as an electro-optic modulator (EOM). The merit of the device is readily determined from the EA signal, without any further characterization, by calculating the overall change in the absorption coefficient given a certain applied field strength. This was recently pointed out in a study by Walters *et al.* wherein EOM device stacks were fabricated by casting MHP nanoplatelets onto an architecture that consisted of a reflective electrode, a MHP layer, a transparent electrode, as well as insulating layers to prevent charge injection from the electrodes into the MHP. The authors found that the absorption change at the peak wavelength was remarkably high at 70 cm^{-1} for a field strength of 56 kV cm^{-1}, representing the largest reported change in absorption coefficient for a solution-processed material at room temperature. Given that the device stack generates field lines perpendicular to the MHP layer, the authors attributed the large changes in the exciton's absorption coefficient to the quantum-confined Stark effect (QCSE) rather than the quadratic Stark effect, i.e., the expected response when fields are applied parallel to the quantum well layers.[92] The quantum-confined Stark effect (QCSE) occurs when a spatially confined system is subjected to an externally applied field along the axis of confinement.[91,92,105-107] The applied field both reduces the bandgap energy and the exciton binding energy resulting in a redshift of the exciton resonance energy that scales quadratically with the applied field strength. Thus, the QCSE is phenomenologically similar to the quadratic Stark effect despite being fundamentally different in physical origin. Inorganic quantum well EOM devices have achieved their highest extinction ratios by exploiting the QCSE.[107]

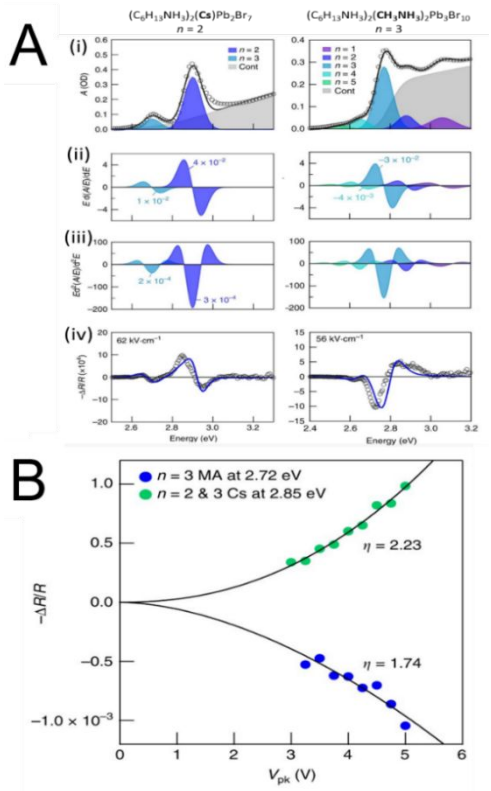

Figure 14. (A) Optical investigations for $(C_6H_{13}NH_3)_2(Cs)Pb_2Br_7$ and $(C_6H_{13}NH_3)_2(CH_3NH_3)_2Pb_3Br_{10}$ thin films. (i) Optical spectra, (ii) first derivative of absorption, (iii) second derivative of absorption, and (iv) EA spectra at indicated applied electric field where the solid lines are fits from transfer matrix modeling of changes to the complex dielectric function of the exciton absorption bands. **(B)** Nonlinear dependence of the QCSE for $(C_6H_{13}NH_3)_2(Cs)Pb_2Br_7$ and $(C_6H_{13}NH_3)_2(CH_3NH_3)_2Pb_3Br_{10}$ thin films. Reproduced with permission from *Nat. Commun.* **2018,** *9*, 4214 (ref. 14). Copyright 2018 Nature.[14]

In addition to characterizing the EOM devices' merit, the EA signals collected by Walters *et al.* also furthered our fundamental understanding of the MHP layer. An anomalous trend was observed in the EA signals of the $(C_6H_{13}NH_3)_2(A)_{n-1}Pb_nBr_{3n+1}$ nanoplatelets when the A-site cation was changed from a Cs^+ atom to the dipolar $CH_3NH_3^+$ molecule, given that the exciton's EA response was inverted (**Figure 14A**). In the case of $(C_6H_{13}NH_3)_2(A)_{n-1}Pb_nBr_{3n+1}$ with A = Cs^+, the exciton absorption peak responded with a redshift expected for the QCSE. However, when A = $CH_3NH_3^+$, the exciton absorption peak is instead blueshifted. The quadratic energy shift in opposite directions is summarized in **Figure 14B** where the $(C_6H_{13}NH_3)_2(A)_{n-1}Pb_nBr_{3n+1}$ with $CH_3NH_3^+$ or Cs^+ display opposing EA amplitude changes at their extrema, representing blue and redshifts,

respectively. The authors complement their EA studies with first-principles DFT calculations to propose a new 'dipole mediated' QCSE. The rotational alignment of the $CH_3NH_3^+$ molecule's dipole parallel with the applied field decreases the exciton binding energy sufficiently to overcome the redshift of the QCSE and even reverse its direction. Overall, this study proves that tunable modulation via cation tailoring is obtainable in MHP nanoplatelet thin films. From a combination of EA and optical absorption spectroscopies, the authors were able to identify blue and redshifts of the excitonic features and identify future materials for electro-optical modulators that possess a unique set of tunable properties.

Experimental challenges of EA spectroscopy

While modulation spectroscopies such as EA produce normalized difference signals (i.e. $\Delta T/T$) that have many inherent advantages and are generally free of any instrument response function, there are still experimental artifacts, challenges, and limitations in EA spectroscopy that interested researchers should be cognizant of. We herein provide a brief summary of common challenges that should be considered when applying EA spectroscopy to MHP systems.

The first category of challenges deals with optical effects that result from differences in sample thickness and measurement geometry, (i.e. reflectance $\Delta R/R$ vs transmission $\Delta T/T$ as well as the angle of the incident radiation). In their EA analysis of the well-known $MAPbI_3$, Ziffer *et al.* found that in the reflection geometry, the line shape of the $\Delta R/R$ signal was sensitive to sample thickness as well as the angle of incident radiation and in some cases, resembled changes in the sample's refractive index Δn more closely than changes in the absorption coefficient $\Delta\alpha$.[10] In contrast, the $\Delta T/T$ signal in a normal-incidence geometry produced consistent, thickness-invariant EA line shapes which closely matched the $\Delta\alpha$ line shape that the authors expected from computational modelling. However, it is still possible for changes in refractive index to influence $\Delta T/T$ signals at normal incidence. Similarly, it is possible for thermal effects, i.e. Joule heating via the electrodes, to influence the EA signal. Therefore, it is recommended that such effects be considered before straightforwardly interpreting EA signals as arising solely from the modulation of the absorption coefficient. For a guide on how to calculate the contribution Δn and Joule heating to the EA signal, we refer readers to the work by Jeglinski and Liess *et al.*.[48,53] In a similar vein, large electric fields can cause dielectric breakdown of the MHP layer and therefore care should be taken to monitor the modulating voltage across the sample with an oscilloscope.

As a second category of challenges, we address the demodulation of the EA signal via lock-in detection. Interested researchers should be aware that a phase shift of π in the input signal will invert the sign of the EA signal, and therefore, the absolute phase of the experimental set up must be rigorously established before assigning meaning to the sign (+/-) of the EA signal. Alternatively, the sign can be assigned if the system's EA response is known beforehand. It should also be noted that lock-in amplifiers detect the RMS amplitude of a single frequency component (i.e. ω or 2ω) within the input signal. Therefore, if the amplitude of the EA spectrum is needed, then it is necessary to multiply the lock-in detected signal by an instrumental correction factor that accounts for the Fourier coefficient of the waveform of the modulating voltage.[90,108] For example, in the case for derivative analysis wherein the ratio between the EA and absorption amplitudes is used to qualitatively determine the excited state's properties, this is a necessary step. Qualitative analysis of the EA signal wherein the field strength F is required can also prove challenging for MHPs. This is because the field strength experienced by excited states will depend on the material's dielectric constant at the frequency of the modulating voltage. Given that MHPs have highly frequency-dependent dielectric functions and experience ion migration effects that depend heavily on sample morphology,[109] obtaining an accurate measurement of the dielectric constant is an additional step that may be challenging for those interested in quantitatively analyzing the EA response of MHPs.

Conclusions and outlook

This review discusses how traditional absorption spectroscopy falls short of characterizing the optoelectronic features of MHPs due to surface artifacts, thin-film coverage, or even spectrometer setup. EA spectroscopy provides a depth of knowledge about charge carrier type and the electric field environment felt by that carrier through simple line shape analysis —information that is often unobtainable by other optical methods. In a similar vein, EA spectroscopy can differentiate between randomly dispersed and well-oriented excitonic features providing a complementary technique to structural characterization. Through changes in the internal electric field, EA spectroscopy can be used to characterize ion migration in MHPs, a crucial hurdle for photovoltaic devices. EA spectroscopy can also be used to deconvolute phase heterogeneities within a thin film, providing critical insight into fundamental material properties to tailor MHPs for highly specific device applications. Overall, EA spectroscopy is a crucial tool for pushing the boundaries of understanding the optoelectronic properties of MHP thin films. When other optical characterizations fall short in the richness of data provided, often times EA spectroscopy can bridge the knowledge gap to afford a complete optoelectronic description of MHPs. The reviewed studies herein have leveraged EA spectroscopy to deepen the fundamental understanding of current complex materials in the form of heterostructures, quantum wells, and/or quantum-confined MHP structures.

As we look into the future of EA spectroscopy, we believe a few crucial areas of interest will be best utilized with this technique. First, there is considerable interest in the field for integrating exotic and optically active π-conjugated organic cations into low dimensional MHP structures.[110-117] These cations have a HOMO/LUMO level near the bandgap of the metal halide lattice, often forming a charge transfer complex at the heterojunction.[112] EA spectroscopy has been used extensively to investigate the optoelectronic properties of charge-transfer complexes in organic semiconductor donor-acceptor systems, such as their large dipole moments or binding energies.[89,118-121] We see EA spectroscopy as a critical tool to fully elucidate the novel charge transfer optoelectronic properties in MHPs as well as for their low dimensional analogs.[112] Second, a promising future application for MHP materials is phase-change memory devices.[122] This requires precise knowledge about the optoelectronic properties at a range of critical temperatures when these phase changes are induced. EA spectroscopy can provide the precision necessary over a range of temperatures while also showing the evolution of new phases.[77] Lastly, there is still considerable work to be done on providing comprehensive models to fit and predict EA features such as FK oscillations, as well as ongoing debates about expected line shapes in the EA spectra of 2D and 3D MHPs. Although the groundwork has been laid, there needs to be a further exploration into these challenges in order to provide a theoretical basis for many complex physical phenomena in MHPs.

Author contributions

The manuscript was written through contributions of all authors. All authors have given approval to the final version of the manuscript.

Conflicts of interest

There are no conflicts to declare.

Acknowledgments

This work was supported by the U.S. Department of Energy, Office of Basic Energy Sciences, Division of Materials Sciences and Engineering under Award no. DE-SC0019041. We would like to thank Prof. Z. Valy Vardeny (ZVV) for valuable discussions on electroabsorption. ZVV would like to acknowledge the support by the DOE under grant no. DE-SC0014579. EA gratefully acknowledges support from the Office of Science Graduate Student Research (SCGSR) fellowship. KH would like to acknowledge support from the National Science Foundation thru Graduate Research Fellowship (Grant No. 1747505). LWB would also like to acknowledge the Sloan Foundation through an Alfred P. Sloan Research Fellowship in Chemistry.

References

(1) Adjokatse, S.; Fang, H.-H.; Loi, M. A. Broadly tunable metal halide perovskites for solid-state light-emission applications. *Mater. Today* **2017**, *20*, 413-424.

(2) Ni, L.; Huynh, U.; Cheminal, A.; Thomas, T. H.; Shivanna, R.; Hinrichsen, T. F.; Ahmad, S.; Sadhanala, A.; Rao, A. Real-time observation of exciton–phonon coupling dynamics in self-assembled hybrid perovskite quantum wells. *ACS Nano* **2017**, *11*, 10834-10843.

(3) Panzer, F.; Li, C.; Meier, T.; Köhler, A.; Huettner, S. Impact of structural dynamics on the optical properties of methylammonium lead iodide perovskites. *Adv. Energy Mater.***2017**, *7*, 1700286.

(4) D'Innocenzo, V.; Grancini, G.; Alcocer, M. J. P.; Kandada, A. R. S.; Stranks, S. D.; Lee, M. M.; Lanzani, G.; Snaith, H. J.; Petrozza, A. Excitons versus free charges in organo-lead tri-halide perovskites. *Nat. Commun.***2014**, *5*, 3586.

(5) Paraecattil, A. A.; De Jonghe-Risse, J.; Pranculis, V.; Teuscher, J.; Moser, J.-E. Dynamics of photocarrier separation in $MAPbI_3$ perovskite multigrain films under a quasistatic electric field. *J. Phys. Chem. C* **2016**, *120*, 19595-19602.

(6) Cheng, Y.; Li, H.-W.; Zhang, J.; Yang, Q.-D.; Liu, T.; Guan, Z.; Qing, J.; Lee, C.-S.; Tsang, S.-W. Spectroscopic study on the impact of methylammonium iodide loading time on the electronic properties in perovskite thin films. *J. Mater. Chem. A* **2016**, *4*, 561-567.

(7) Kim, H.; Zhao, L.; Price, J. S.; Grede, A. J.; Roh, K.; Brigeman, A. N.; Lopez, M.; Rand, B. P.; Giebink, N. C. Hybrid perovskite light emitting diodes under intense electrical excitation. *Nat. Commun.* **2018**, *9*, 4893.

(8) Guo, Y.; Jia, Y.; Li, N.; Chen, M.; Hu, S.; Liu, C.; Zhao, N. Degradation mechanism of perovskite light-emitting diodes: An in situ investigation via electroabsorption spectroscopy and device modelling. *Adv. Funct. Mater.* **2020**, *30*, 1910464.

(9) Bouduban, M. E. F.; Burgos-Caminal, A.; Teuscher, J.; Moser, J.-E. Unveiling the nature of charge carrier interactions by electroabsorption spectroscopy: An illustration with lead-halide perovskites. *Chimia* **2017**, *71*, 231-235.

(10) Ziffer, M. E.; Mohammed, J. C.; Ginger, D. S. Electroabsorption spectroscopy measurements of the exciton binding energy, electron–hole reduced effective mass, and band gap in the perovskite $CH_3NH_3PbI_3$. *ACS Photonics* **2016**, *3*, 1060-1068.

(11) Hong, X.; Ishihara, T.; Nurmikko, A. V. Dielectric confinement effect on excitons in PbI_4-based layered semiconductors. *Phys. Rev. B* **1992**, *45*, 6961-6964.

(12) Ruf, F.; Magin, A.; Schultes, M.; Ahlswede, E.; Kalt, H.; Hetterich, M. Excitonic nature of optical transitions in electroabsorption spectra of perovskite solar cells. *Appl. Phys. Lett.* **2018**, *112*, 083902.

(13) Tanaka, K.; Kondo, T. Bandgap and exciton binding energies in lead-iodide-based natural quantum-well crystals. *Sci. Technol. Adv. Mater.* **2003,** *4*, 599-604.

(14) Walters, G.; Wei, M.; Voznyy, O.; Quintero-Bermudez, R.; Kiani, A.; Smilgies, D. M.; Munir, R.; Amassian, A.; Hoogland, S.; Sargent, E. The quantum-confined Stark effect in layered hybrid perovskites mediated by orientational polarizability of confined dipoles. *Nat. Commun.***2018**, *9*, 4214.

(15) Tanaka, K.; Sano, F.; Takahashi, T.; Kondo, T.; Ito, R.; Ema, K. Two-dimensional Wannier excitons in a layered-perovskite-type crystal $(C_6H_{13}NH_3)_2PbI_4$. *Solid State Commun.* **2002**, *122*, 249-252.

(16) Awasthi, K.; Du, K.-B.; Wang, C.-Y.; Tsai, C.-L.; Hamada, M.; Narra, S.; Diau, E. W.-G.; Ohta, N. Electroabsorption studies of multicolored lead halide perovskite nanocrystalline solid films. *ACS Photonics* **2018**, *5*, 2408-2417.

(17) Tanaka, K.; Takahashi, T.; Kondo, T.; Umeda, K.; Ema, K.; Umebayashi, T.; Asai, K.; Uchida, K.; Miura, N. Electronic and excitonic structures of inorganic–organic perovskite-type quantum-well crystal $(C_4H_9NH_3)_2PbBr_4$. *Jpn. J. Appl. Phys.* **2005,** *44*, 5923-5932.

(18) Koutselas, I. B.; Ducasse, L.; Papavassiliou, G. C. Electronic properties of three- and low-dimensional semiconducting materials with Pb halide and Sn halide units. *J. Phys: Condens. Matter* **1996,** *8*, 1217-1227.

(19) Zhai, Y.; Baniya, S.; Zhang, C.; Li, J.; Haney, P.; Sheng, C.-X.; Ehrenfreund, E.; Vardeny, Z. V. Giant Rashba splitting in 2D organic-inorganic halide perovskites measured by transient spectroscopies. *Sci. Adv.* **2017**, *3*, e1700704.

(20) Takagi, H.; Kunugita, H.; Ema, K. Influence of the image charge effect on excitonic energy structure in organic-inorganic multiple quantum well crystals. *Phys. Rev. B* **2013**, *87*, 125421.

(21) Kattoor, V.; Awasthi, K.; Jokar, E.; Diau, E. W.-G.; Ohta, N. Integral method analysis of electroabsorption spectra and electrophotoluminescence study of $(C_4H_9NH_3)_2PbI_4$ organic–inorganic quantum well. *J. Phys. Chem. C* **2018,** *122*, 26623-26634.

(22) Rana, S.; Awasthi, K.; Bhosale, S. S.; Diau, E. W.-G.; Ohta, N. Temperature-dependent electroabsorption and electrophotoluminescence and exciton binding eEnergy in $MAPbBr_3$ perovskite quantum dots. *J. Phys. Chem. C* **2019,** *123*, 19927-19937.

(23) Kim, M.-c.; Ham, S.-Y.; Cheng, D.; Wynn, T. A.; Jung, H. S.; Meng, Y. S. Advanced characterization techniques for overcoming challenges of perovskite solar cell materials. *Adv. Energy Mater.* **2021,** *11*, 2001753.

(24) Tian, Y.; Scheblykin, I. G. Artifacts in absorption measurements of organometal halide perovskite materials: what are the real spectra? *J. Phys. Chem. Lett.* **2015,** *6*, 3466-3470.

(25) Tauc, J.; Grigorovici, R.; Vancu, A. Optical properties and electronic structure of amorphous germanium. *Phys. Status Solidi B* **1966,** *15*, 627-637.

(26) Davis, E. A.; Mott, N. F. Conduction in non-crystalline systems V. Conduction in non-crystalline systems V. Conductivity, optical absorption and photoconductivity in

amorphous semiconductors. *Philos. Mag.: A Journal of Theoretical Experimental and Applied Physics* **1970,** *22*, 0903-0922.

(27) Pankove, J. I.; Kiewit, D. A. Optical processes in semiconductors. *J. Electrochem. Soc.* **1972,** *119*, 156C.

(28) Tauc, J. Optical properties and electronic structure of amorphous Ge and Si. *Mater. Res. Bull.* **1968,** *3*, 37-46.

(29) Zanatta, A. R. Revisiting the optical bandgap of semiconductors and the proposal of a unified methodology to its determination. *Sci. Rep.* **2019**, *9*, 11225.

(30) Fox, M. Optical properties of solids. *Am. J. Phys.* **2002,** *70*, 1269-1270.

(31) Blancon, J. C.; Stier, A. V.; Tsai, H.; Nie, W.; Stoumpos, C. C.; Traoré, B.; Pedesseau, L.; Kepenekian, M.; Katsutani, F.; Noe, G. T.; Kono, J.; Tretiak, S.; Crooker, S. A.; Katan, C.; Kanatzidis, M. G.; Crochet, J. J.; Even, J.; Mohite, A. D. Scaling law for excitons in 2D perovskite quantum wells. *Nat. Commun.* **2018**, *9*, 2254.

(32) Mehdizadeh-Rad, H.; Singh, J. Influence of Urbach Energy, Temperature, and longitudinal position in the active layer on carrier diffusion length in perovskite solar cells. *ChemPhysChem* **2019,** *20*, 2712-2717.

(33) Viezbicke, B. D.; Patel, S.; Davis, B. E.; Birnie Iii, D. P. Evaluation of the Tauc method for optical absorption edge determination: ZnO thin films as a model system. *Phys. Status Solidi B* **2015,** *252*, 1700-1710.

(34) Ledinsky, M.; Schönfeldová, T.; Holovský, J.; Aydin, E.; Hájková, Z.; Landová, L.; Neyková, N.; Fejfar, A.; De Wolf, S. Temperature dependence of the Urbach energy in lead iodide perovskites. *J. Phys. Chem. Lett.* **2019,** *10*, 1368-1373.

(35) Chen, X.; Lu, H.; Yang, Y.; Beard, M. C. Excitonic effects in methylammonium lead halide perovskites. *J. Phys. Chem. Lett.* **2018,** *9*, 2595-2603.

(36) Baranowski, M.; Plochocka, P. Excitons in metal-halide perovskites. *Adv. Energy Mater.* **2020**, *10*, 1903659.

(37) Mahboubi Soufiani, A.; Yang, Z.; Young, T.; Miyata, A.; Surrente, A.; Pascoe, A.; Galkowski, K.; Abdi-Jalebi, M.; Brenes, R.; Urban, J.; Zhang, N.; Bulović, V.; Portugall, O.; Cheng, Y.-B.; Nicholas, R. J.; Ho-Baillie, A.; Green, M. A.; Plochocka, P.; Stranks, S. D. Impact of microstructure on the electron–hole interaction in lead halide perovskites. *Energy Environ. Sci.* **2017,** *10*, 1358-1366.

(38) Sell, D. D. Resolved free-exciton transitions in the optical-absorption spectrum of GaAs. *Phys. Rev. B* **1972**, *6*, 3750-3753.

(39) Phuong, L. Q.; Yamada, Y.; Nagai, M.; Maruyama, N.; Wakamiya, A.; Kanemitsu, Y. Free carriers versus excitons in $CH_3NH_3PbI_3$ perovskite thin films at low temperatures: charge transfer from the orthorhombic phase to the tetragonal phase. *J. Phys. Chem. Lett.* **2016,** *7*, 2316-2321.

(40) Jiang, Y.; Wang, X.; Pan, A. Properties of excitons and photogenerated charge carriers in metal halide perovskites. *Adv. Mater.* **2019,** *31*, 1806671.

(41) Manser, J. S.; Kamat, P. V. Band filling with free charge carriers in organometal halide perovskites. *Nat. Photonics* **2014**, *8*, 737-743.

(42) Deschler, F.; Price, M.; Pathak, S.; Klintberg, L. E.; Jarausch, D.-D.; Higler, R.; Hüttner, S.; Leijtens, T.; Stranks, S. D.; Snaith, H. J.; Atatüre, M.; Phillips, R. T.; Friend, R. H. High photoluminescence efficiency and optically pumped lasing in solution-processed mixed halide perovskite semiconductors. *The J. Phys. Chem. Lett.* **2014**, *5*, 1421-1426.

(43) Even, J.; Pedesseau, L.; Katan, C. Analysis of multivalley and multibandgap absorption and enhancement of free carriers related to exciton screening in hybrid perovskites. *J. Phys. Chem. C* **2014**, *118*, 11566-11572.

(44) Elliott, R. J. Intensity of optical absorption by excitons. *Phys. Rev.* **1957**, *108*, 1384-1389.

(45) Galkowski, K.; Mitioglu, A.; Miyata, A.; Plochocka, P.; Portugall, O.; Eperon, G. E.; Wang, J. T.-W.; Stergiopoulos, T.; Stranks, S. D.; Snaith, H. J.; Nicholas, R. J. Determination of the exciton binding energy and effective masses for methylammonium and formamidinium lead tri-halide perovskite semiconductors. *Energy Environ. Sci.* **2016,** *9*, 962-970.

(46) Aspnes, D. E. Third-derivative modulation spectroscopy with low-field electroreflectance. *Surf. Sci.* **1973**, *37*, 418-442.

(47) Amerling, E.; Baniya, S.; Lafalce, E.; Zhang, C.; Vardeny, Z. V.; Whittaker-Brooks, L. Electroabsorption spectroscopy studies of $(C_4H_9NH_3)_2PbI_4$ organic–inorganic hybrid perovskite multiple quantum wells. *J. Phys. Chem. Lett.* **2017,** *8*, 4557-4564.

(48) Liess, M.; Jeglinski, S.; Vardeny, Z. V.; Ozaki, M.; Yoshino, K.; Ding, Y.; Barton, T. Electroabsorption spectroscopy of luminescent and nonluminescent pi-conjugated polymers. *Phys. Rev. B* **1997,** *56*, 15712-15724.

(49) Bublitz, G. U.; Boxer, S. G. Stark Spectroscopy: Applications in chemistry, biology, and materials science. *Annu. Rev. Phys. Chem.* **1997,** *48*, 213-242.

(50) de Sa Pereira, D.; Menelaou, C.; Danos, A.; Marian, C.; Monkman, A. P. Electroabsorption spectroscopy as a tool for probing charge transfer and state mixing in thermally activated delayed fluorescence emitters. *J. Phys. Chem. Lett.* **2019,** *10*, 3205-3211.

(51) Sebastian, L.; Weiser, G.; Bässler, H. Charge transfer transitions in solid tetracene and pentacene studied by electroabsorption. *Chem. Phys.* **1981**, *61*, 125-135.

(52) Liptay, W. Dipole moments and polarizabilities of molecules in excited electronic states. In *Excited States*, Lim, E. C., Ed. Elsevier 1974; Vol. 1, pp 129-229.

(53) Jeglinski, S. A.; Vardeny, Z. V.; Ding, Y.; Barton, T. Electroabsorption and charged-excitation spectroscopy of pi-conjugated polymers. Mol. Cryst. Liq. Cryst. Scie. Technol. A **1994,** *256*, 87-96.

(54) Liptay, W. Electrochromism and Solvatochromism. *Angew. Chem. Int. Ed.* **1969,** *8*, 177-188.

(55) Horvath, A.; Weiser, G.; Baker, G. L.; Etemad, S. Influence of disorder on the field-modulated spectra of polydiacetylene films. *Phys. Rev. B* **1995**, *51*, 2751-2758.

(56) Dow, J. D.; Redfield, D. Electroabsorption in semiconductors: The excitonic absorption edge. *Phys. Rev. B* **1970**, *1*, 3358-3371.

(57) Kneissl, M.; Linder, N.; Kiesel, P.; Quassowski, S.; Schmidt, K.; Döhler, G. H.; Grothe, H.; Smith, J. S. Two-dimensional Franz-Keldysh effect in MQW structures with lateral electric fields. *Superlattices Microstruct.* **1994,** *16*, 109.

(58) Shanabrook, B. V.; Glembocki, O. J.; Beard, W. T. Photoreflectance modulation mechanisms in $GaAs/Al_xGa_{1-x}As$ multiple quantum wells. *Phys. Rev. B* **1987,** *35*, 2540-2543.

(59) Shen, H.; Dutta, M. Franz–Keldysh oscillations in modulation spectroscopy. *J. Appl. Phys.* **1995**, *78*, 2151-2176.

(60) Gerhard, W.; Horvath, A.; Kolbe, H. J. In *Franz-Keldysh effect of band states in polydiacetylene*, Proc.SPIE1997.

(61) Pollak, F. H. Modulation spectroscopy of semiconductor microstructures. *Superlattices Microstruct.* **1991,** *10*, 333-346.

(62) Jaeger, A.; Weiser, G. Excitonic electroabsorption spectra and Franz-Keldysh effect of $In_{0.53}Ga_{0.47}As$/InP studied by small modulation of static fields. *Phys. Rev. B* **1998,** *58*, 10674-10682.

(63) Cardona, M.: Modulation spectroscopy of semiconductors. In *Festkörperprobleme 10: Plenary Lectures of the Professional Groups "Semiconductor Physics", "Low Temperature Physics", "Thermodynamics", "Metal Physics" of the German Physical Society Freudenstadt, April 6–11, 1970*, Madelung, O., Ed. Springer Berlin Heidelberg: Berlin, Heidelberg, 1970; pp 125-173.

(64) Heesel, H.; Hunsche, S.; Mikkelsen, H.; Dekorsy, T.; Leo, K.; Kurz, H. Dynamics of electric field screening in a bulk GaAs modulator. *Phys. Rev. B* **1993**, *47*, 16000-16003.

(65) Thouin, F.; Valverde-Chávez, D. A.; Quarti, C.; Cortecchia, D.; Bargigia, I.; Beljonne, D.; Petrozza, A.; Silva, C.; Srimath Kandada, A. R. Phonon coherences reveal the polaronic character of excitons in two-dimensional lead halide perovskites. *Nat. Mater.***2019**, *18*, 349-356.

(66) Wright, A. D.; Verdi, C.; Milot, R. L.; Eperon, G. E.; Pérez-Osorio, M. A.; Snaith, H. J.; Giustino, F.; Johnston, M. B.; Herz, L. M. Electron–phonon coupling in hybrid lead halide perovskites. *Nat. Commun.* **2016**, *7*, 11755.

(67) Wang, F.; Bai, S.; Tress, W.; Hagfeldt, A.; Gao, F. Defects engineering for high-performance perovskite solar cells. *npj Flexible Electronics* **2018**, *2*, 22.

(68) Zhang, X.; Turiansky, M. E.; Van de Walle, C. G. Correctly assessing defect tolerance in halide perovskites. *J. Phys. Chem. C* **2020,** *124*, 6022-6027.

(69) Huang, H.; Bodnarchuk, M. I.; Kershaw, S. V.; Kovalenko, M. V.; Rogach, A. L. Lead halide perovskite nanocrystals in the research spotlight: stability and defect tolerance. *ACS Energy Lett.* **2017,** *2*, 2071-2083.

(70) Meggiolaro, D.; Motti, S. G.; Mosconi, E.; Barker, A. J.; Ball, J.; Andrea Riccardo Perini, C.; Deschler, F.; Petrozza, A.; De Angelis, F. Iodine chemistry determines the defect tolerance of lead-halide perovskites. *Energy Environ. Sci.* **2018**, *11*, 702-713.

(71) Blancon, J. C.; Tsai, H.; Nie, W.; Stoumpos, C. C.; Pedesseau, L.; Katan, C.; Kepenekian, M.; Soe, C. M. M.; Appavoo, K.; Sfeir, M. Y.; Tretiak, S.; Ajayan, P. M.; Kanatzidis, M. G.; Even, J.; Crochet, J. J.; Mohite, A. D. Extremely efficient internal exciton dissociation through edge states in layered 2D perovskites. *Science* **2017**, *355*, 1288.

(72) Aspnes, D. E. Electric field effects on the dielectric constant of solids. *Phys. Rev.* **1967**, *153*, 972-982.

(73) Aspnes, D. E.; Rowe, J. E. Resonant nonlinear optical susceptibility: Electroreflectance in the low-field limit. *Phys. Rev. B* **1972**, *5*, 4022-4030.

(74) Sebastian, L.; Weiser, G. One-dimensional wide energy bands in a polydiacetylene revealed by electroreflectance. *Phys. Rev. Lett.* **1981**, *46*, 1156-1159.

(75) Fraschini, E.; Bonati, L.; Pitea, D. Molecular polarizability as a tool for understanding the binding properties of polychlorinated dibenzo-p-dioxins: definition of a reliable computational procedure. *J. Phys. Chem.* **1996,** *100*, 10564-10569.

(76) Xu, C.-q.; Fukuta, S. y.; Sakakura, H.; Kondo, T.; Ito, R.; Takahashi, Y.; Kumata, K. Anomalous electro-absorption in the low-temperature phase of $(C_{10}H_{21}NH_3)_2PbI_4$. *Solid State Commun.* **1991,** *77*, 923-926.

(77) Yu, P. Y.; Cardona, M. Effect of quantum confinement on electrons and phonons in semiconductors. In *Fundamentals of Semiconductors: Physics and Materials Properties*, Yu, P. Y.; Cardona, M., Eds. Springer Berlin Heidelberg: Berlin, Heidelberg, 2010; pp 469-551.

(78) Burkhard, G. F.; Hoke, E. T.; McGehee, M. D. Accounting for interference, scattering, and electrode absorption to make accurate internal quantum efficiency measurements in organic and other thin solar cells. *Adv. Mater.* **2010**, *22*, 3293-3297.

(79) Liu, J.; Leng, J.; Wang, S.; Zhang, J.; Jin, S. Artifacts in transient absorption measurements of perovskite films induced by transient reflection from morphological microstructures. *J. Phys. Chem. Lett.* **2019**, *10*, 97-101.

(80) Manzoor, S.; Häusele, J.; Bush, K. A.; Palmstrom, A. F.; Carpenter, J.; Yu, Z. J.; Bent, S. F.; McGehee, M. D.; Holman, Z. C. Optical modeling of wide-bandgap perovskite and perovskite/silicon tandem solar cells using complex refractive indices for arbitrary-bandgap perovskite absorbers. *Opt. Express* **2018,** *26*, 27441-27460.

(81) Lee, J.; Rovira, P. I.; An, I.; Collins, R. W. Rotating-compensator multichannel ellipsometry: Applications for real time Stokes vector spectroscopy of thin film growth. *Rev. Sci. Instrum.* **1998,** *69*, 1800-1810.

(82) Diroll, B. T. Temperature-dependent intraband relaxation of hybrid perovskites. *J. Phys. Chem. Lett.* **2019**, *10*, 5623-5628.

(83) Blossey, D. F. Wannier exciton in an electric field. II. Electroabsorption in direct-band-gap solids. *Phys. Rev. B* **1971,** *3*, 1382-1391.

(84) Dow, J. D.; Lao, B. Y.; Newman, S. A. Differential electroabsorption. *Phys. Rev. B* **1971**, *3*, 2571-2581.

(85) Pham, M. T.; Amerling, E.; Luong, H. M.; Pham, H. T.; Larsen, G. K.; Whittaker-Brooks, L.; Nguyen, T. D. Origin of Rashba spin-orbit coupling in 2D and 3D lead iodide perovskites. *Sci. Rep.* **2020**, *10*, 4964.

(86) Amerling, E.; Baniya, S.; Lafalce, E.; Blair, S.; Vardeny, Z. V.; Whittaker-Brooks, L. Quantifying exciton heterogeneities in mixed-phase organometal halide multiple quantum wells via Stark spectroscopy studies. *ACS Appl. Mater. Interfaces* **2020,** *12*, 52538-52548.

(87) Yin, J.; Li, H.; Cortecchia, D.; Soci, C.; Brédas, J.-L. Excitonic and polaronic properties of 2D hybrid organic–inorganic perovskites. *ACS Energy Lett.* **2017**, *2*, 417-423.

(88) Veldhuis, S. A.; Boix, P. P.; Yantara, N.; Li, M.; Sum, T. C.; Mathews, N.; Mhaisalkar, S. G. Perovskite materials for light-emitting diodes and lasers. *Adv. Mater.* **2016**, *28*, 6804-6834.

(89) Weiser, G. Stark effect of one-dimensional Wannier excitons in polydiacetylene single crystals. *Phys. Rev. B* **1992**, *45*, 14076-14085.

(90) Hansen, K. R.; McClure, C. E.; Colton, J. S.; Whittaker-Brooks, L. Franz-Keldysh and Stark effects in two-dimensional metal halide perovskites. **2021**, *arXiv:2109.09021v1*

(91) Miller, D. A. B.; Chemla, D. S.; Damen, T. C.; Gossard, A. C.; Wiegmann, W.; Wood, T. H.; Burrus, C. A. Band-edge electroabsorption in quantum well structures: The quantum-confined Stark effect. *Phys. Rev. Lett.* **1984**, *53*, 2173-2176.

(92) Miller, D. A. B.; Chemla, D. S.; Damen, T. C.; Gossard, A. C.; Wiegmann, W.; Wood, T. H.; Burrus, C. A. Electric field dependence of optical absorption near the band gap of quantum-well structures. *Phys. Rev. B* **1985**, *32*, 1043-1060.

(93) Campbell, I. H.; Ferraris, J. P.; Hagler, T. W.; Joswick, M. D.; Parker, I. D.; Smith, D. L. Measuring internal electric fields in organic light-emitting diodes using electroabsorption spectroscopy. *Polym. Adv. Technol.* **1997,** *8*, 417-423.

(94) Futscher, M. H.; Lee, J. M.; McGovern, L.; Muscarella, L. A.; Wang, T.; Haider, M. I.; Fakharuddin, A.; Schmidt-Mende, L.; Ehrler, B. Quantification of ion migration in $CH_3NH_3PbI_3$

perovskite solar cells by transient capacitance measurements. *Mater. Horiz.* **2019**, *6*, 1497-1503.

(95) Calado, P.; Telford, A. M.; Bryant, D.; Li, X.; Nelson, J.; O'Regan, B. C.; Barnes, P. R. F. Evidence for ion migration in hybrid perovskite solar cells with minimal hysteresis. *Nat. Commun.* **2016**, *7*, 13831.

(96) Li, Z.; Xiao, C.; Yang, Y.; Harvey, S. P.; Kim, D. H.; Christians, J. A.; Yang, M.; Schulz, P.; Nanayakkara, S. U.; Jiang, C.-S.; Luther, J. M.; Berry, J. J.; Beard, M. C.; Al-Jassim, M. M.; Zhu, K. Extrinsic ion migration in perovskite solar cells. *Energy Environ. Sci.* **2017**, *10*, 1234-1242.

(97) Kim, S.-Y.; Yang, J.-M.; Choi, E.-S.; Park, N.-G. Layered $(C_6H_5CH_2NH_3)_2CuBr_4$ perovskite for multilevel storage resistive switching memory. *Adv. Funct. Mater.* **2020,** *30*, 2002653.

(98) Han, J. S.; Le, Q. V.; Choi, J.; Kim, H.; Kim, S. G.; Hong, K.; Moon, C. W.; Kim, T. L.; Kim, S. Y.; Jang, H. W. Lead-free all-inorganic cesium tin iodide perovskite for filamentary and interface-type resistive switching toward environment-friendly and temperature-tolerant nonvolatile memories. *ACS Appl. Mater. Interfaces* **2019,** *11*, 8155-8163.

(99) Zheng, K.; Chen, Y.; Sun, Y.; Chen, J.; Chábera, P.; Schaller, R.; Al-Marri, M. J.; Canton, S. E.; Liang, Z.; Pullerits, T. Inter-phase charge and energy transfer in Ruddlesden–Popper 2D perovskites: critical role of the spacing cations. *J. Mater. Chem. A* **2018**, *6*, 6244-6250.

(100) Williams, O. F.; Guo, Z.; Hu, J.; Yan, L.; You, W.; Moran, A. M. Energy transfer mechanisms in layered 2D perovskites. *J. Chem. Phys.* **2018,** *148*, 134706.

(101) Quan, L. N.; Zhao, Y.; García de Arquer, F. P.; Sabatini, R.; Walters, G.; Voznyy, O.; Comin, R.; Li, Y.; Fan, J. Z.; Tan, H.; Pan, J.; Yuan, M.; Bakr, O. M.; Lu, Z.; Kim, D. H.; Sargent, E. H. Tailoring the energy landscape in quasi-2D halide perovskites enables efficient green-light emission. *Nano Lett.* **2017,** *17*, 3701-3709.

(102) Shang, Q.; Wang, Y.; Zhong, Y.; Mi, Y.; Qin, L.; Zhao, Y.; Qiu, X.; Liu, X.; Zhang, Q. Unveiling structurally engineered carrier dynamics in hybrid quasi-two-dimensional perovskite thin films toward controllable emission. *J. Phys. Chem. Lett.* **2017,** *8*, 4431-4438.

(103) Ithurria, S.; Tessier, M. D.; Mahler, B.; Lobo, R. P. S. M.; Dubertret, B.; Efros, A. L. Colloidal nanoplatelets with two-dimensional electronic structure. *Nat. Mater.***2011**, *10*, 936-941.

(104) Wu, X.; Yu, H.; Li, L.; Wang, F.; Xu, H.; Zhao, N. Composition-dependent light-induced dipole moment change in organometal halide perovskites. *J. Phys. Chem. C* **2015,** *119*, 1253-1259.

(105) Weiner, J. S.; Miller, D. A. B.; Chemla, D. S. Quadratic electro-optic effect due to the quantum-confined Stark effect in quantum wells. *Appl. Phys. Lett.* **1987**, *50*, 842-844.

(106) Lever, L.; Ikonić, Z.; Valavanis, A.; Cooper, J. D.; Kelsall, R. W. Design of Ge–SiGe quantum-confined Stark effect electroabsorption heterostructures for CMOS compatible photonics. *J. Lightwave Technol.* **2010,** *28*, 3273-3281.

(107) Rouifed, M. S.; Chaisakul, P.; Marris-Morini, D.; Frigerio, J.; Isella, G.; Chrastina, D.; Edmond, S.; Roux, X. L.; Coudevylle, J.-R.; Vivien, L. Quantum-confined Stark effect at 1.3 μm in $Ge/Si_{0.35}Ge_{0.65}$ quantum-well structure. *Opt. Lett.* **2012,** *37*, 3960-3962.

(108) Jeglinski, S. A. Electroabsorption spectroscopy of conjugated polymers and carbon fullerenes and conjugated-polymer light-emitting devices. *Ph. D. Thesis, University of Utah* **1996**.

(109) Flannery, L.; Ogle, J.; Powell, D.; Tassone, C.; Whittaker-Brooks, L. Voltage bias stress effects in metal halide perovskites are strongly dependent on morphology and ion migration pathways. *J. Mater. Chem. A* **2020**, *8*, 25109-25119.

(110) Liu, J.-J.; Guan, Y.-F.; Jiao, C.; Lin, M.-J.; Huang, C.-C.; Dai, W.-X. A panchromatic hybrid crystal of iodoplumbate nanowires and J-aggregated naphthalene diimides with long-lived charge-separated states. *Dalton Trans.* **2015**, *44*, 5957-5960.

(111) Proppe, A. H.; Tremblay, M.-H.; Zhang, Y.; Yang, Z.; Quintero-Bermudez, R.; Kelley, S. O.; Barlow, S.; Marder, S. R.; Sargent, E. H. Naphthalenediimide cations inhibit 2D perovskite formation and facilitate subpicosecond electron transfer. *J. Phys. Chem. C* **2020,** *124*, 24379-24390.

(112) Amerling, E.; Zhai, Y.; Larson, B. W.; Yao, Y.; Fluegel, B.; Owczarczyk, Z.; Lu, H.; Whittaker-Brooks, L.; Blum, V.; Blackburn, J. L. Charge transfer states and carrier generation in 1D organolead iodide semiconductors. *J. Mater. Chem. A* **2021**, *9*, 14977-14990.

(113) Gélvez-Rueda, M. C.; Fridriksson, M. B.; Dubey, R. K.; Jager, W. F.; van der Stam, W.; Grozema, F. C. Overcoming the exciton binding energy in two-dimensional perovskite nanoplatelets by attachment of conjugated organic chromophores. *Nat. Commun.* **2020**, *11*, 1901.

(114) Passarelli, J. V.; Mauck, C. M.; Winslow, S. W.; Perkinson, C. F.; Bard, J. C.; Sai, H.; Williams, K. W.; Narayanan, A.; Fairfield, D. J.; Hendricks, M. P.; Tisdale, W. A.; Stupp, S. I. Tunable exciton binding energy in 2D hybrid layered perovskites through donor–acceptor interactions within the organic layer. *Nat. Chem.***2020**, *12*, 672-682.

(115) Van Gompel, W. T. M.; Herckens, R.; Van Hecke, K.; Ruttens, B.; D'Haen, J.; Lutsen, L.; Vanderzande, D. Towards 2D layered hybrid perovskites with enhanced functionality: introducing charge-transfer complexes via self-assembly. *Chem. Commun.* **2019**, *55*, 2481-2484.

(116) Jana, M. K.; Liu, C.; Lidin, S.; Dirkes, D. J.; You, W.; Blum, V.; Mitzi, D. B. Resolving rotational stacking disorder and electronic level alignment in a 2D oligothiophene-based lead iodide perovskite. *Chem. Mater.* **2019**, *31*, 8523-8532.

(117) Dunlap-Shohl, W. A.; Barraza, E. T.; Barrette, A.; Dovletgeldi, S.; Findik, G.; Dirkes, D. J.; Liu, C.; Jana, M. K.; Blum, V.; You, W.; Gundogdu, K.; Stiff-Roberts, A. D.; Mitzi, D. B. Tunable internal quantum well alignment in rationally designed oligomer-based perovskite films deposited by resonant infrared matrix-assisted pulsed laser evaporation. *Mater. Horiz.* **2019**, *6*, 1707-1716.

(118) Devižis, A.; De Jonghe-Risse, J.; Hany, R.; Nüesch, F.; Jenatsch, S.; Gulbinas, V.; Moser, J.-E. Dissociation of charge transfer states and carrier separation in bilayer organic solar cells: A time-resolved electroabsorption spectroscopy study. *J. Am. Chem. Soc.* **2015**, *137*, 8192-8198.

(119) Kazaoui, S.; Minami, N.; Tanabe, Y.; Byrne, H. J.; Eilmes, A.; Petelenz, P. Comprehensive analysis of intermolecular charge-transfer excited states in C_{60} and C_{70} films. *Phys. Rev. B* **1998,** *58*, 7689-7700.

(120) Rohwer, E. J.; Akbarimoosavi, M.; Meckel, S. E.; Liu, X.; Geng, Y.; Lawson Daku, L. M.; Hauser, A.; Cannizzo, A.; Decurtins, S.; Stanley, R. J.; Liu, S.-X.; Feurer, T. Dipole moment and polarizability of tunable intramolecular charge transfer states in heterocyclic π-conjugated molecular dyads determined by computational and Stark spectroscopic study. *J. Phys. Chem. C* **2018,** *122*, 9346-9355.

(121) Gélinas, S.; Rao, A.; Kumar, A.; Smith, S. L.; Chin, A. W.; Clark, J.; van der Poll, T. S.; Bazan, G. C.; Friend, R. H. Ultrafast

long-range charge separation in organic semiconductor photovoltaic diodes. *Science* **2014**, *343*, 512.

(122) Zou, C.; Zheng, J.; Chang, C.; Majumdar, A.; Lin, L. Y. Nonvolatile rewritable photomemory arrays based on reversible phase-change perovskite for optical information storage. *Adv. Opt. Mater.* **2019**, *7*, 1900558.

Biographies

Eric Amerling

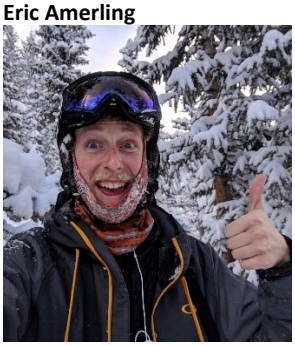

Eric Amerling obtained his Ph.D from the Chemistry Department at the University of Utah. From 2019 to 2020, he was working at NREL as a DOE SCGSR fellow. His research interests include the structural and optoelectronic properties of low-dimensional materials.

Kameron Hansen

Kameron Hansen is an NSF Graduate Research Fellow in the Chemistry Department at the University of Utah. His research interests are centered on investigating the optical properties of two-dimensional perovskites and transition metal dichalcogenides.

Luisa Whittaker-Brooks

Luisa Whittaker-Brooks is an Associate Professor of Chemistry at the University of Utah. Her research centers on the design of well-defined hybrid materials with controlled morphology and interfaces that serve as conduits for deterministic and coherent energy and charge transfer for applications in *energy conversion, storage, and electronics.* She received her B.S. in Chemistry from The University of Panama. Under a Fulbright Fellowship, she received her Ph.D. in Chemistry from the University at Buffalo. She was a postdoctoral researcher at Princeton University under a L'Oréal for Women in Science Fellowship.